# A Riemann–Hilbert problem for the finite-genus solutions of the KdV equation and its numerical solution

Thomas Trogdon[1] and Bernard Deconinck

Department of Applied Mathematics
University of Washington
Campus Box 352420
Seattle, WA, 98195, USA

July 29, 2012

**Abstract**

We derive a Riemann–Hilbert problem satisfied by the Baker-Akhiezer function for the finite-gap solutions of the Korteweg-de Vries (KdV) equation. As usual for Riemann-Hilbert problems associated with solutions of integrable equations, this formulation has the benefit that the space and time dependence appears in an explicit, linear and computable way. We make use of recent advances in the numerical solution of Riemann–Hilbert problems to produce an efficient and uniformly accurate numerical method for computing all periodic and quasi-periodic finite-genus solutions of the KdV equation.

## 1 Introduction

The goal of this paper is to find a new description for the so-called finite-genus or finite-gap solutions of the Korteweg-de Vries (KdV) equation

$$u_t + 6uu_x + u_{xxx} = 0, \quad (x,t) \in \mathbb{R} \times \mathbb{R}, \tag{1.1}$$

and to use this description to compute them.

The finite-genus solutions arise in the spectral analysis of the Schrödinger operator with periodic or quasi-periodic potential, where the spectrum has only a finite number $g$ of finite-length bands separated by $g$ gaps. They are explicitly described in terms of Riemann theta functions, parameterized by hyperelliptic compact Riemann surfaces of genus $g$. In the context of the periodic problem for (1.1), these solutions play the same role that is played by trigonometric polynomials for the linear KdV equation $u_t + u_{xxx} = 0$ of (1.1): the general solution to the periodic problem in the space of square-integrable functions is approximated arbitrarily close by a finite-genus solution with sufficiently high $g$. An eloquent overview of the extensive literature on these solutions is found in McKean's review [14] of [15]. Of particular importance in the development of this literature are the pioneering works of Lax [13] and Novikov [18]. Excellent reviews are also found in Chapter 2 of [17], Dubrovin's oft-cited review article [9], and [2], parts of which focus specifically on the computation of these solutions.

The computation of the finite-genus solutions is a nontrivial matter. Although Lax's original paper [13] includes an appendix by Hyman, where solutions of genus 2 were obtained through a variational principle, the now-standard approach of their computation goes through their algebro-geometric description in terms of Riemann surfaces, see [4] or [12], for instance. Another approach is through the numerical solution of the so-called Dubrovin equations, a set of coupled ordinary differential equations that describe the dynamics of the zeros and poles of an auxiliary eigenfunction of the spectral problem, the Baker-Akhiezer function

[1]Corresponding author, email: trogdon@amath.washington.edu

[2, 8]. The finite-genus solution is easily recovered from the solution of the Dubrovin equations [17, 22]. One advantage of all these approaches over the variational method employed by Lax and Hyman is that periodic and quasi-periodic solutions are constructed with equal ease. The same is true for our approach, described below.

The essence of this paper is the derivation of a Riemann–Hilbert representation of the Baker–Akhiezer function. We construct a Riemann–Hilbert problem (RHP) whose solution is used to find the Baker–Akhiezer function. From this, one extracts the associated solution of the KdV equation. The $x$- and $t$-dependence of the solution appear in an explicit way, so that no time or space stepping is required to obtain the value of the solution at a specific $x$ and $t$. This should be contrasted with, for instance, the numerical solution of the Dubrovin equations [22]. Furthermore, just like for the method of inverse scattering [24], the infinite-line counterpart of the problem under investigation, this dependence of the KdV solution on its independent variables appears linearly in an exponential function in the RHP.

In order to solve this RHP, we employ a regularization procedure using a $g$-function [7]. This simplifies the $x$ and $t$ dependence further. The resulting RHP has piecewise constant jumps. Straightforward modifications allow the RHP to be numerically solved efficiently using the techniques in [20]. This results in an approximation of the Baker–Akhiezer function that is uniformly valid on its associated Riemann surface. This, in turn, produces a uniform approximation of the associated solution of the KdV equation in the entire $(x, t)$ plane.

In this paper, we begin by introducing the required fundamentals from the theory of Riemann surfaces. Next we use the methods of Chapter 2 of [17] to describe how hyperelliptic Riemann surfaces are used to solve the KdV equation for a restricted class of initial conditions. The representation of the Baker–Akhiezer function in terms of a RHP is derived in the next section. The modification of this RHP is discussed in the two subsequent sections. The final form of the RHP is presented in Section 6. In the final section the RHP is solved numerically and the numerical convergence of the method is verified. The method is illustrated there with many numerical examples.

It is unlikely that this new computational approach to the finite-genus solutions of the KdV equation is competitive in terms of speed, with the classical approach via Riemann theta functions and Riemann surfaces cited above. Nevertheless, the explicit description of these solutions in terms of a RHP and its numerical solution may lead to other interesting developments. Furthermore, through the results of [21], the accuracy of the numerical results is guaranteed for all ranges of the parameters.

## 2 Riemann surfaces

We use this section to introduce the fundamental ideas from the theory of Riemann surfaces that are needed below. Most of these fundamental facts can be found in [2, 8]. The unfinished lecture notes by B. A. Dubrovin [10] provide an especially readable introduction and most results stated below can also be found there.

**Definition 2.1.** *Let*

$$F(\lambda, \mu) = \mu^2 - P_{2g+2}(\lambda), \text{ or } F(\lambda) = \mu^2 - P_{2g+1}(\lambda).$$

*The algebraic curve associated with this function is the solution set in $\mathbb{C}^2$ of the equation $F(\lambda, w) = 0$. The desingularization and compactification of this curve is a Riemann surface, $\Gamma$. For this restricted class of polynomials the associated Riemann surface $\Gamma$ is said to be hyperelliptic. We only consider hyperelliptic surfaces.*

Define the $a$ cycles $\{a_j\}_{j=1}^g$ and the $b$ cycles $\{b_j\}_{j=1}^g$ on the Riemann surface as in Figure 1. The set $\{a_j \cup b_j\}_{j=1}^g$ is a basis for the homology of the Riemann surface. It is well known that the hyperelliptic surfaces in Definition 2.1 are of genus $g$; they can be identified with a sphere with $g$ handles. It is also well known that a genus $g$ surface has $g$ linearly independent holomorphic differentials, denoted $\omega_1, \ldots \omega_g$. We choose the normalization

$$\oint_{a_j} \omega_k = 2\pi i \delta_{jk}, \quad j, k = 1, \ldots, g.$$

The matrix

$$\boldsymbol{B} = (B_{jk})_{1\le j,k\le g}\,, \quad B_{jk} = \oint_{b_j} \omega_k,$$

is known as a Riemann matrix. Although this matrix has important properties and is necessary for computing the theta function representation of the finite-genus solutions we do not need it directly.

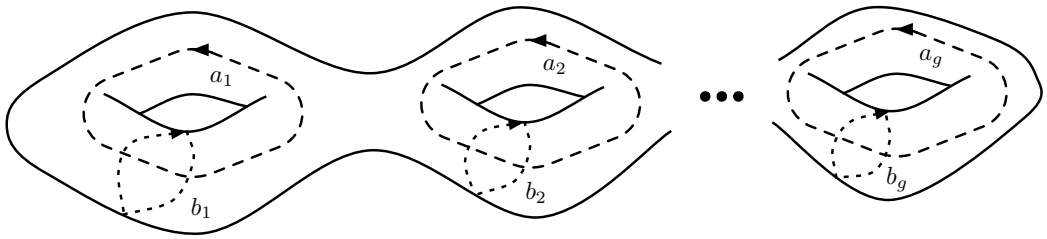


Figure 1: A cartoon of a hyperelliptic Riemann surfaces with a choice for the $a$ and $b$ cycles.

**Lemma 2.1** ([9])**.** *Let $\omega$ be a holomorphic differential on a Riemann surfaces of genus $g$. If*

$$\oint_{a_j} \omega = 0,\ j = 1, \ldots, g,$$

*then $\omega = 0$.*

**Lemma 2.2** ([9])**.** *Every holomorphic differential $f$ on a genus $g$ hyperelliptic Riemann surface $\mu^2 - P_{2g+1}(\lambda) = 0$ can be expressed locally as*

$$f = \frac{q(\lambda)}{\mu} d\lambda,$$

*where $q$ is a polynomial of degree at most $g-1$.*

A divisor is a formal sum

$$D = \sum_{j=1}^{k} n_j Q_j, \quad n_j \in \mathbb{Z},$$

of points $Q_j$ on the Riemann surface. Given a meromorphic function $f$ on the Riemann surface with poles at $Q_j$ of multiplicity $n_j$ and zeros at $R_j$ with multiplicity $m_j$ we define the associated divisor

$$(f) = \sum_{j=1}^{l} m_j R_j - \sum_{j=1}^{k} n_j Q_j.$$

The degree of a divisor

$$\deg D = \sum_{j=1}^{k} n_j \text{ so that } \deg(f) = \sum_{j=1}^{k} n_j - \sum_{j=1}^{l} m_i.$$

A divisor is said to be positive if each $n_j$ is positive and $D > D'$ holds if $D - D'$ is positive. We use $l(D)$ to denote the dimension of the space of meromorphic functions $f$ such that $(f) \ge D$.

**Lemma 2.3** (Riemann inequality [9])**.** *For a genus $g$ surface, if $\deg D \ge g$ then*

$$l(D) \ge 1 + \deg D - g.$$

A divisor $D$ is said to be nonspecial if the Riemann inequality is an equality. Define the Abel mapping for points on the Riemann surface by

$$A(Q) = \left[ \begin{array}{ccc} \int_{Q_0}^{Q} \omega_1 & \cdots & \int_{Q_0}^{Q} \omega_g \end{array} \right], \tag{2.1}$$

where the path of integration is taken to be the same for all integrals. Note that this is well-defined for the appropriately normalized differentials. We extend this map to divisors $D = \sum_{j=1}^{k} n_j Q_j$ by

$$A(D) = \sum_{j=1}^{k} n_j A(Q_j).$$

**Theorem 2.1** ([9]). *The Abel map $A$ maps points on the symmetrized Riemann surface to the associated Jacobi variety $J(\Gamma) = \mathbb{C}^g/\{2\pi M + BN\}$ for $M, N \in \mathbb{Z}^g$. Furthermore, if the divisor $D = Q_1 + \cdots + Q_g$ is nonspecial then $A$ has a single-valued inverse from the Jacobi variety to the symmetrized Riemann surface in a neighborhood of $A(D)$.*

We do not make use of this theorem directly but include it for completeness. Next, we describe properties of Abelian differentials of the second kind that are needed below

**Definition 2.2.** *Given a point $Q$ on the Riemann surface and a positive integer $n$, an Abelian differential of the second kind is a meromorphic differential that has a single pole of order $n+1$, so that its local representation is*

$$\nu_Q^n = \left(z^{-n-1} + \mathcal{O}(1)\right) dz,$$

*with respect to a local parameter $z$, $z(Q) = 0$.*

When $Q$ is the point at infinity we construct these differentials explicitly. As a local parameter we take $z^2 = 1/\lambda$ since $Q$ is a branch point. If $n$ is even we set

$$\nu_\infty^n = -\frac{1}{2}\lambda^{n/2-1} d\lambda.$$

When $n$ is odd, there is more to be done. First, compute

$$\frac{\lambda^j}{w} d\lambda = -2\frac{z^{-2j-3}}{\sqrt{P(z^{-2})}} dz.$$

Then

$$P(z^{-2}) = z^{-4g-2}(1 - z^2\alpha_{g+1}) \prod_{j=1}^{g} (1 - z^2\alpha_j)(1 - z^2\beta_j).$$

Thus

$$\begin{aligned} \frac{\lambda^j}{w} d\lambda &= -2z^{-2j-2+2g} \left( (1 - z^2\alpha_{g+1}) \prod_{j=1}^{g} (1 - z^2\alpha_j)(1 - z^2\beta_j) \right)^{-1/2} dz \\ &= (-2z^{-2j-2+2g} + \mathcal{O}(1)) dz. \end{aligned}$$

We choose $j = g + (n-1)/2$ so that

$$\nu_\infty^n = -\frac{1}{2} \frac{\lambda^{g+(n-1)/2}}{w} d\lambda.$$

Let $\mu_\infty^n$ be the differential obtained from $\nu_\infty^n$ by adding holomorphic differentials so that it has zero $a$ cycles. We state a lemma concerning the $b$-periods of these differentials.

**Lemma 2.4** ([10]). *Define $y_k(z)$ through the equality $\omega_k = y_k(z)dz$ and $z^2 = 1/\lambda$. Then*

$$\oint_{b_k} \mu_\infty^n = \frac{1}{n!} \frac{d^{n-1}}{dz^{n-1}} y_k(z) \bigg|_{z=0}, \quad k = 1, \ldots, g.$$

# 3 The finite-genus solutions of the KdV equation

We begin by considering the scattering problem associated with the KdV equation. The time-independent Schrödinger equation

$$-\Psi_{xx} - u_0(x)\Psi = \lambda\Psi, \tag{3.1}$$

is solved for eigenfunctions $\Psi(x,\lambda)$ bounded for all $x$. We define the Bloch spectrum

$$\mathcal{S}(u_0) = \left\{ \lambda \in \mathbb{C} : \text{ there exists a solution such that } \sup_{x\in\mathbb{R}} |\Psi(x,\lambda)| < \infty \right\}.$$

It is well known that for $u_0(x)$ smooth and periodic the Bloch spectrum consists of a countable collection of real intervals

$$\mathcal{S}(u_0) = \bigcup_{j=1}^{\infty} [\alpha_j, \beta_j],$$
$$\alpha_j < \beta_j < \alpha_{j+1} < \beta_{j+1}.$$

If there are only $n+1$ intervals then $\beta_{n+1} = \infty$. We refer to the intervals $[\alpha_j, \beta_j]$ as bands and the intervals $[\beta_j, \alpha_{j+1}]$ as gaps.

**Assumption 3.1.** *$\mathcal{S}(u_0)$ consists of a finite number of intervals. In this case we say that $u_0$ is a finite gap potential.*

Define $\Gamma$ to be the hyperelliptic Riemann surface associated with the function

$$F(\lambda,\mu) = \mu^2 - P(\lambda), \quad P(\lambda) = (\lambda - \alpha_{g+1}) \prod_{j=1}^{g} (\lambda - \alpha_j)(\lambda - \beta_j).$$

See Figure 2 for a cartoon. We divide this surface into two sheets. Choose the branch cuts for the function $\sqrt{P(\lambda)}$ along $\mathcal{S}(u_0)$. We fix the branch by the requirement $\sqrt{P(\lambda)} \sim (-1)^g i|\lambda|^{g+1/2}$ as $\lambda \to -\infty$. Define $\sqrt{P(\lambda)}^{+}$ to be the value $\lim_{\epsilon\to 0^+} \sqrt{P(\lambda + i\epsilon)}$. This allows us to define

$$\Gamma_{\pm} = \{(\lambda, \pm\sqrt{P(\lambda)}^{+}) : \lambda \in \mathbb{C}\}.$$

When considering a function $f$ defined on $\Gamma$ we use the notation $f_{\pm}$ so that $f_+(f_-)$ denotes the function restricted to $\Gamma_+(\Gamma_-)$. In this way we can consider $f_{\pm}$ as a function of only $\lambda$. We need an explicit description of the $a$ cycles since we take a computational approach below:

$$a_i = \{(\lambda, \sqrt{P(\lambda)}^{+}) : \lambda \in (\beta_i, \alpha_{i+1}]\} \cup \{(\lambda, -\sqrt{P(\lambda)}^{+}) : \lambda \in [\beta_i, \alpha_{i+1})\}.$$

The $a_i$ component on $\Gamma_+(\Gamma_-)$ is oriented in the direction of decreasing(increasing) $\lambda$. This description is also useful since we will consider poles and zeros lying on the $a$ cycles.

**Remark 3.1.** *There is some inconsistency in the notation $f_{\pm}$ which is also present in the literature [10]. In what follows, it will be clear from context whether we are referring to a function defined on the Riemann surface or to $f_+$ and $f_-$ separately.*

We introduce further notation that will be of use later. Given a point $Q = (\lambda, w) \in \Gamma$, we follow [11] and define the involution $*$ by $Q^* = (\lambda, -w)$. This is an isomorphism from one sheet of the Riemann surface to the other. It is clear the first sheet is isomorphic to the cut plane

$$\hat{\mathbb{C}} = \mathbb{C} \setminus \left\{ [\alpha_{g+1}, \infty) \cup \bigcup_{j=1}^{g} [\alpha_j, \beta_j] \right\},$$

through the mapping $\hat{} : \Gamma_+ \to \hat{\mathbb{C}}$ defined by $\hat{Q} = \lambda$ and its inverse $\check{} : \hat{\mathbb{C}} \to \Gamma_+$ defined by $\check{\lambda} = (\lambda, \sqrt{P(\lambda)}^{+})$.

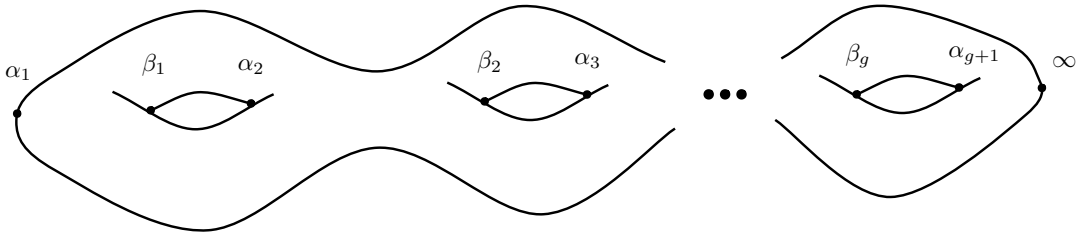


Figure 2: A cartoon of the Riemann surface associated with the finite gap potential $u_0$.

**Lemma 3.1.** *[17] For every $x_0 \in \mathbb{R}$ there exist two solutions $\Psi_\pm$ of (3.1) such that*

- *$\Psi_\pm(x,\lambda)$ is meromorphic on $\Gamma \setminus \{\infty\}$ with $g$ poles at*

$$D = \sum_{i=1}^{g} Q_i, \quad Q_i \in a_i,$$

*and $g$ zeros at*

$$D' = \sum_{i=1}^{g} R_i, \quad R_i \in a_i.$$

- *Define $\gamma_i = \hat{R}_i$ then $\{\gamma_j\}_{j=1}^g$ satisfies*

$$\gamma_j(x_0) \in [\beta_j, \alpha_{j+1}], \tag{3.2}$$

$$\gamma_j' = -\frac{2i\sqrt{P(\gamma_j)}}{\prod_{k\neq j}(\gamma_j - \gamma_k)}. \tag{3.3}$$

- *$\Psi_\pm(x,\lambda) = e^{\pm i\sqrt{\lambda}(x-x_0)}(1+\mathcal{O}(\lambda^{-1/2}))$ as $\lambda \to \infty$.*

For simplicity we take $x_0 = 0$ below. We will always take the branch cut for $\lambda^{1/2}$ to be along $[0,\infty)$ and fix the branch by $\lambda^{1/2} \sim i|\lambda|^{1/2}$ as $\lambda \to -\infty$. If the potential $u_0(x)$ is taken as an initial condition for the KdV equation then these zeros have both time and space dependence $\gamma_j = \gamma_j(x,t)$. This dependence is given by [8]

$$\dot{\gamma}_j = -\frac{8i(\gamma_j + u_0/2)\sqrt{P(\gamma_j)}}{\prod_{k\neq j}(\gamma_j - \gamma_k)}, \tag{3.4}$$

and the solution to the KdV equation can be reconstructed through

$$u(x,t) = -2\sum_{j=1}^{g} \gamma_j(x,t) + \alpha_{g+1} + \sum_{j=1}^{g}(\alpha_j + \beta_j).$$

The (now time-dependent) function $\Psi_\pm(x,t,\lambda)$ is known as a Baker–Akhiezer (BA) function. From the general theory of Baker–Akhiezer functions [17] it is known that it is uniquely determined by a nonspecial divisor

$$D = \sum_{i=1}^{g} Q_i,$$

for the poles and the asymptotic behavior [17]. The following lemma shows that all divisors we consider are nonspecial.

**Lemma 3.2.** *On the hyperelliptic surface $\mu^2 = P(\lambda)$ the divisor $D = \sum_{i=1}^{g} R_i$, where $R_i \in a_i$ is nonspecial.*

Proof. *Assume $f$ is meromorphic with $D \leq (f)$. The differential $w = df$ has double poles with zero residues at the points $R_i$. We have the following representation*

$$w = \sum_{i=1}^{g} y_i + \eta.$$

*Here $y_i$ are Abelian differentials of the second kind normalized so that they have zero periods along the a cycles and second-order poles at the points $R_i$. Since $f$ is single valued on the Riemann surface*

$$\oint_{a_k} w = 0, \quad \oint_{b_k} w = 0, \quad k = 1, \dots, g.$$

*Since the a periods vanish we conclude that $\eta$ has zero a periods and must be zero. From the b period condition we obtain*

$$\oint_{b_k} w = \sum_{j=1}^{g} c_j \psi_{kj}(z_j(0)) = 0, \tag{3.5}$$

*where $z_j$ is a local parameter near $R_j = z_j(0)$ and $\psi_{kj}$ is determined from the equality $\omega_k = \psi_{kj}(z_j)dz_j$ near $R_j$. We know that $\omega_k$ can be expressed uniquely as the sum of differentials of the form*

$$u_l = \frac{\lambda^{l-1}}{\mu} d\lambda, \text{ for } l = 1, \dots, g,$$

*with coefficients $d_{kl}$. If $R_j = (z_j, \pm\sqrt{P(z_j)})$ is not a branch point we obtain*

$$\psi_{k,j}(z_j) = \sum_{l=1}^{g} d_{kj} \frac{z_j^{l-1}}{\sqrt{P(z_j)}}.$$

*If it is a branch point $R_j = (z_j, 0)$ we use the local parameter $s = \sqrt{\lambda - z_j}$ so that*

$$\psi_{k,j}(z_j) = \sum_{l=1}^{g} d_{kl} \frac{2z_j^{l-1}}{\sqrt{P'(z_j)}}.$$

*Since the matrix $\boldsymbol{d}_{kl}$ is invertible the condition* (3.5) *is reduced to the study of the matrix*

$$\boldsymbol{Z}_{jl} = z_j^{l-1},$$

*after multiplying rows by suitable constants. This is a Vandermonde matrix, and thus invertible. This shows that $c_j = 0$ and thus $w = 0$ and $f = C \in \mathbb{C}$. This proves the result.* ■

**Remark 3.2.** *We have shown that the Abel map is invertible from the Jacobi variety to the symmeterized Riemann surface in a neighborhood of $A(D)$ for every divisor we consider.*

Being precise, we obtain the following unique characterization of the function $\Psi_{\pm}(x, t, \lambda)$ [17]:

**Definition 3.1.** *The BA function for the solution of the KdV with initial condition $u_0(x)$ is the unique function that satisfies*

- $\Psi_{\pm}$ *solves* (3.1).
- $\Psi_{\pm}$ *is meromorphic on $\Gamma \setminus \{\infty\}$ with poles at*

$$D = \sum_{i=1}^{g} Q_i, \quad Q_i \in a_i, \quad \hat{Q}_i = \gamma_i(0, 0). \tag{3.6}$$

- $\Psi_\pm(x,t,\lambda) = e^{\pm i\lambda^{1/2}x \pm 4i\lambda^{3/2}t}(1+\mathcal{O}(\lambda^{-1/2}))$ *as* $\lambda\to\infty$.
- $u_0(x) = -2\sum_{j=1}^g \gamma_j(x,0) + \alpha_{g+1} + \sum_{j=1}^g(\alpha_j+\beta_j)$.

**Remark 3.3.** *Instead of computing the zeros of the BA function we derive a Riemann–Hilbert formulation of the BA function to compute the function itself. The main benefit of this approach is that the roles of $x$ and $t$ in the problem are reduced to that of parameters. This gives an approximation to the solution of the KdV equation that is uniformly convergent in the $(x,t)$ plane. In this sense our method is comparable to the theta function approach which can also achieve uniform convergence [12]. On the other hand, no time stepping is required, as for the direct numerical solution of the PDE or the numerical solution of 3.2 and 3.4.*

In what follows we assume without loss of generality that $\alpha_1 = 0$. If $\alpha_1 \neq 0$ we define $\tau = \lambda - \alpha_1$ and consider a modified scattering problem

$$-\Psi_{xx} - u_0(x)\Psi = (\tau+\alpha_1)\Psi, \tag{3.7}$$
$$-\Psi_{xx} - \tilde{u}_0(x)\Psi = \tau\Psi,\ \tilde{u}_0(x) = u_0(x)+\alpha_1. \tag{3.8}$$

Let $u(x,t)$ and $\tilde{u}(x,t)$ be the solutions of the KdV equation with $u_0(x)$ and $\tilde{u}_0(x)$ respectively, as initial conditions. If $\tilde{u}(x,t)$ satisfies the KdV equation then so does $\tilde{u}(x-6ct,t)+c$. Therefore, by uniqueness, $u(x,t) = \tilde{u}(x+6\alpha_1 t,t) - \alpha_1$.

# 4 From a Riemann surface of genus $g$ to the cut plane

Consider the hyperelliptic Riemann surface $\Gamma$ from Section 3. We represent a function $f_\pm$ defined on $\Gamma$ by a vector-valued function $\boldsymbol{f}$ on $\hat{\mathbb{C}}$ by

$$\boldsymbol{f}(\lambda) = \begin{bmatrix} f_+(\check{\lambda}) & f_-((\check{\lambda})^*) \end{bmatrix}.$$

Assume the function $f_\pm$ is continuous on all of $\Gamma$. Let $\lambda\in(\alpha_j,\beta_j)$ and define $\lambda_{\pm\epsilon} = \lambda \pm i\epsilon$. It follows that $\lim_{\epsilon\to0^+}\check{\lambda}_{\pm\epsilon} = \lim_{\epsilon\to0^+}(\check{\lambda}_{\mp\epsilon})^*$. From the continuity of $f_\pm$

$$\lim_{\epsilon\to0^+} f_+(\check{\lambda}_{\pm\epsilon}) = \lim_{\epsilon\to0^+} f_-((\check{\lambda}_{\mp\epsilon})^*).$$

Let $\boldsymbol{f}^\pm(\lambda) = \lim_{\epsilon\to0^+}\boldsymbol{f}(\lambda\pm i\epsilon)$. Then

$$\boldsymbol{f}^+(\lambda) = \boldsymbol{f}^-(\lambda)\begin{bmatrix} 0 & 1 \\ 1 & 0 \end{bmatrix}.$$

We form a planar representation of the BA function

$$\boldsymbol{\Psi}(\lambda) = \begin{bmatrix} f_+(\check{\lambda}) & f_-((\check{\lambda})^*) \end{bmatrix}.$$

The function $\boldsymbol{\Psi}$ satisfies

$$\boldsymbol{\Psi}^+(x,t,\lambda) = \boldsymbol{\Psi}^-(x,t,\lambda)\begin{bmatrix} 0 & 1 \\ 1 & 0 \end{bmatrix},\ \lambda\in(\alpha_{n+1},\infty)\cup\bigcup_{j=1}^g(\alpha_j,\beta_j),$$
$$\boldsymbol{\Psi}(x,t,\lambda) = \begin{bmatrix} e^{i\lambda^{1/2}x+4i\lambda^{3/2}} & e^{-i\lambda^{1/2}x-4i\lambda^{3/2}} \end{bmatrix}(I+\mathcal{O}(\lambda^{-1/2})).$$

The next step is to remove the oscillatory nature of $\boldsymbol{\Psi}$ for large $\lambda$. This procedure will affect the jumps, thus some care is in order. Define

$$\boldsymbol{R}(x,t,\lambda) = \begin{bmatrix} e^{-\zeta(x,t,\lambda)/2} & 0 \\ 0 & e^{\zeta(x,t,\lambda)/2} \end{bmatrix},$$
$$\zeta(x,t,\lambda) = 2ix\lambda^{1/2} + 8it\lambda^{3/2}$$

The function $\mathbf{\Phi}(x,t,\lambda) = \Psi(x,t,\lambda)\boldsymbol{R}(x,t,\lambda)$ satisfies

$$\begin{aligned}
\mathbf{\Phi}^+(x,t,\lambda) &= \mathbf{\Phi}^-(x,t,\lambda)\begin{bmatrix} 0 & 1 \\ 1 & 0 \end{bmatrix},\ \lambda \in (\alpha_{n+1},\infty) \cup \bigcup_{j=1}^{g}(\alpha_j,\beta_j),\\
\mathbf{\Phi}^+(x,t,\lambda) &= \mathbf{\Phi}^-(x,t,\lambda)\begin{bmatrix} e^{-\zeta(x,t,\lambda)} & 0 \\ 0 & e^{\zeta(x,t,\lambda)} \end{bmatrix},\ \lambda \in \bigcup_{j=1}^{g}(\beta_j,\alpha_{j+1}),\\
\mathbf{\Phi}(x,t,\lambda) &= \begin{bmatrix} 1 & 1 \end{bmatrix}(I + \mathcal{O}(\lambda^{-1/2})).
\end{aligned} \tag{4.1}$$

This is a RHP for $\mathbf{\Phi}$ when the poles at $\gamma_j(0,0)$ coincide with $\alpha_j$ or $\beta_j$. The boundary values of the solution to the RHP should be at least locally integrable [11]. A pole at a band end ($\alpha_j$ or $\beta_j$) corresponds to a square-root singularity. In general, we have poles in the intervals $(\beta_j,\alpha_{j+1})$ where there are smooth jumps. In Section 5.1 we treat the case where $\gamma_j(0,0) = \beta_j$, $j = 1,\dots,g$ while enforcing that $\mathbf{\Phi}$ remains bounded at $\{\alpha_j\}_{j=1}^g$. No such enforcement is made at $\{\beta_j\}_{j=1}^g$. The general case of poles on the $a$ cycles is treated in Section 5.2.

# 5 Regularization

We show how the jump conditions in (4.1) can be reduced to piecewise constant jumps. As mentioned above, we first perform the calculations in the simpler case when the poles are located at $(\beta_j,0)$ on $\Gamma$. In the general case, we use an additional BA function as a parametrix to move the poles to the band ends thus reducing the problem to the first case.

## 5.1 All poles at the band ends

We assume $\gamma_j(0,0) = \beta_j$. Define the $g$-function

$$\mathcal{G}(x,t,\lambda) = \frac{\sqrt{P(\lambda)}}{2\pi i}\sum_{j=1}^{g}\int_{\beta_j}^{\alpha_{j+1}} \frac{-\zeta(x,t,s) + i\Omega_j(x,t)}{\sqrt{P(s)}^+}\frac{ds}{s-\lambda}, \tag{5.1}$$

where $\Omega_j(x,t)$ is constant in $\lambda$ and will be determined below.

**Lemma 5.1.** *The $g$-function satisfies*

- $\mathcal{G}^+(x,t,\lambda) + \mathcal{G}^-(x,t,\lambda) = 0$ *for* $\lambda \in (\alpha_j,\beta_j)$,
- $\mathcal{G}^+(x,t,\lambda) - \mathcal{G}^-(x,t,\lambda) = -\zeta(x,t,\lambda) + i\Omega_j(x,t)$ *for* $\lambda \in (\beta_j,\alpha_{j+1})$,
- $\mathcal{G}(x,t,\lambda)/\sqrt{P(\lambda)} = \sum_{k=1}^{g} m_k(x,t)\lambda^{-k} + \mathcal{O}(\lambda^{-g-1})$ *as* $\lambda \to \infty$ *where*

$$m_k(x,t) = -\frac{1}{2\pi i}\sum_{j=1}^{g}\int_{\beta_j}^{\alpha_{j+1}} \frac{-\zeta(x,t,s) + i\Omega_j(x,t)}{\sqrt{P(s)}^+}s^{k-1}ds.$$

Proof: *The first two properties follow from the branching properties of $\sqrt{P(\lambda)}$ and properties of Cauchy integrals. The last property follows from expanding $1/(s-\lambda)$ in a Neumann series for large $\lambda$.* ■

Define the matrix function

$$\boldsymbol{G}(x,t,\lambda) = \begin{bmatrix} e^{-\mathcal{G}(x,t,\lambda)} & 0 \\ 0 & e^{\mathcal{G}(x,t,\lambda)} \end{bmatrix},$$

and consider the function

$$\mathbf{\Sigma}(x,t,\lambda) = \mathbf{\Phi}(x,t,\lambda)\boldsymbol{G}(x,t,\lambda).$$

Using Lemma 5.1 we compute the jumps of $\mathbf{\Sigma}$:

$$\mathbf{\Sigma}^+(x,t,\lambda) = \mathbf{\Sigma}^-(x,t,\lambda) \begin{bmatrix} 0 & 1 \\ 1 & 0 \end{bmatrix}, \ \lambda \in (\alpha_{g+1}, \infty) \cup \bigcup_{j=1}^{g} (\alpha_j, \beta_j), \tag{5.2}$$

$$\mathbf{\Sigma}^+(x,t,\lambda) = \mathbf{\Sigma}^-(x,t,\lambda) \begin{bmatrix} e^{i\Omega_j(x,t)} & 0 \\ 0 & e^{-i\Omega_j(x,t)} \end{bmatrix}, \ \lambda \in \bigcup_{j=1}^{g} (\beta_j, \alpha_{j+1}). \tag{5.3}$$

Since $\sqrt{P(\lambda)} = \mathcal{O}(|\lambda|^{g+1/2})$, $\boldsymbol{G}$ has growth in $\lambda$ at $\infty$ unless $m_k(x,t) = 0$ for $k = 1, \dots, g$. We wish to determine $\{\Omega_j\}_{j=1}^g$ so that $\mathbf{\Sigma}$ has the same asymptotic behavior as $\mathbf{\Phi}$ as $\lambda \to \infty$, see 4.1. Thus, we must solve the following problem which we put in slightly more abstract terms since we make use of it again below.

**Problem 5.1** (The Moment Problem)**.** *Given continuous functions*

$$f_j(\lambda) : [\beta_j, \alpha_{j+1}] \to \mathbb{C}, \quad j = 1, \dots, g,$$

*we seek constants $\Omega_j$ satisfying the moment conditions*

$$0 = \int_{\beta_j}^{\alpha_{j+1}} \frac{-f_j(\lambda) + i\Omega_j}{\sqrt{P(\lambda)}^+} \lambda^{i-1} d\lambda, \quad j = 1, \dots, g.$$

**Theorem 5.1.** *The Moment Problem has a unique solution. Further, if each $f_j$ takes purely imaginary values then each $\Omega_j$ is real valued.*

Proof: *The second claim follows from the fact that $\sqrt{P(\lambda)}^+$ takes purely imaginary values in the gaps, $[\beta_j, \alpha_{j+1}]$. To establish the first claim, notice that the Moment Problem is equivalent to the linear system*

$$\begin{aligned} &\boldsymbol{M\Omega} = \boldsymbol{V}, \\ &\boldsymbol{M}_{kj} = i \int_{\beta_j}^{\alpha_{j+1}} \frac{\lambda^{k-1}}{\sqrt{P(\lambda)}} d\lambda, \\ &\boldsymbol{\Omega}_j = \Omega_j, \quad \boldsymbol{V}_i = \sum_{j=1}^{g} \int_{\beta_j}^{\alpha_{j+1}} \frac{f_j(\lambda)}{\sqrt{P(\lambda)}} \lambda^{k-1} d\lambda. \end{aligned}$$

*Assume the rows of $M$ are linearly dependent. Then there exist constants $d_k$ such that*

$$\sum_{k=1}^{g} d_k \boldsymbol{M}_{kj} = 0, \ \textit{for } j = 1, \dots, g.$$

*Explicitly, this implies*

$$\sum_{k=1}^{g} \int_{\beta_j}^{\alpha_{j+1}} \frac{d_k}{\sqrt{P(\lambda)}} \lambda^{k-1} d\lambda = \int_{\beta_j}^{\alpha_{j+1}} \left( \sum_{k=1}^{g} d_k \lambda^{k-1} \right) \frac{d\lambda}{\sqrt{P(\lambda)}}, \ \textit{for } j = 1, \dots, g.$$

*We show this implies that the holomorphic differential*

$$f = \sum_{k=1}^{g} d_k \lambda^{k-1} \frac{d\lambda}{\sqrt{P(\lambda)}} = \sum_{k=1}^{g} d_k \lambda^{k-1} \frac{d\lambda}{w},$$

*has zero a periods. Compute*

$$\int_{\alpha_j}^{\beta_{j+1}} \frac{\lambda^{k-1}}{w} d\lambda = \frac{1}{2} \left( \int_{\alpha_j}^{\beta_{j+1}} \frac{\lambda^{k-1}}{w} d\lambda + \int_{\beta_{j+1}}^{\alpha_j} \frac{\lambda^{k-1}}{-w} d\lambda \right) = \frac{1}{2} \oint_{a_j} \frac{\lambda^{k-1}}{w} d\lambda.$$

*Indeed, $f$ integrates to zero around every a cycle implying that $f$ is the zero differential, see Lemma 2.1. But since each of $\lambda^{k-1} w^{-1} d\lambda$ is linearly independent we conclude that $d_k = 0$, $k = 1, \dots, g$ and the rows of $\boldsymbol{M}$ are linearly independent. The Moment Problem is uniquely solvable.* ■

If we select $\Omega_j$ to make all $m_k$ vanish we use the condition

$$\lim_{\lambda\to\infty} \mathbf{\Sigma}(x,t,\lambda) = \left[\begin{array}{cc} 1 & 1 \end{array}\right],$$

in conjunction with (5.2) to obtain a RHP for $\mathbf{\Sigma}$. It is important that $\mathbf{\Omega}$ in Problem 5.1 is real valued. This implies the piecewise-constant jump matrix in (5.2) is bounded for all $x$ and $t$.

## 5.2 Poles in the gaps

In this section we show how to use an additional BA function to, in effect, reduce the case where $\gamma_j(0,0) \in (\beta_j, \alpha_{j+1})$ to that of $\gamma_j(0,0) = \beta_j$. We assume that not all poles of $\Psi_\pm$ lie on the band ends $\{\beta_j\}_{j=1}^g$. Consider the planar representation of a BA function $(\Psi_p)_\pm$ which satisfies

$$\begin{aligned}
\mathbf{\Psi}_p^+(x,t,\lambda) &= \mathbf{\Psi}_p^-(x,t,\lambda)\left[\begin{array}{cc} 0 & 1 \\ 1 & 0 \end{array}\right],\ \lambda \in (\alpha_{g+1},\infty) \cup \bigcup_{j=1}^g (\alpha_j,\beta_j), \\
\mathbf{\Psi}_p(x,t,\lambda) &= \left[\begin{array}{cc} e^{\kappa(\lambda)/2} & e^{-\kappa(\lambda)/2} \end{array}\right](I + \mathcal{O}(\lambda^{-1/2})), \\
\kappa(\lambda) &= \sum_{j=1}^g i t_j \lambda^{j-1/2}, \quad t_j \in \mathbb{R},
\end{aligned}$$

with poles at $\beta_j$. The goal is to choose $\{t_j\}_{j=1}^g$ so that $(\Psi_p)_\pm$ has zeros precisely at the poles of $\Psi_\pm$. Define $(\Psi_r)_\pm = \Psi_\pm(\Psi_p)_\pm$. The planar representation $\mathbf{\Psi}_r = \mathbf{\Psi}\mathbf{\Psi}_p$ with entry-wise multiplication will now have poles at $\beta_j$ and zeros at the zeros of $\mathbf{\Psi}$. We find $\Psi_\pm$ by first finding two functions $(\Psi_p)_\pm$ and $(\Psi_r)_\pm$ both of which have poles at $\{(0,\beta_j)\}_{j=1}^g$ and dividing. Thus, the general case of poles in gaps is reduced to poles at band ends provided we can find the required $\{t_j\}_{j=1}^g$.

**Remark 5.1.** *We are using the term poles loosely. On $\hat{\mathbb{C}}$, $\mathbf{\Psi}_p$ has unbounded square-root singularities while on $\Gamma$, $(\Psi_p)\pm$ has poles.*

We show that we can choose $\{t_j\}_{j=1}^g$ so that the zeros of $(\Psi_p)_\pm$ will be at an arbitrary divisor

$$D' = \sum_{j=1}^g R_j, \quad R_j \in a_j.$$

We first state a lemma about the location of the zeros and poles of a BA function.

**Lemma 5.2.** *[2] Let $D'$ be the divisor of the zeros of the BA function and $D$ be that of the poles. Assume*

$$\Psi_\pm(\lambda) = e^{q(k)}(1 + \mathcal{O}(k^{-1})), \quad k \to \infty, \quad k^2 = \lambda. \tag{5.4}$$

*On the Jacobi variety $J(\Gamma)$*

$$A(D') = A(D) - \boldsymbol{V}, \tag{5.5}$$

*where $\boldsymbol{V}$ is the vector of the b-periods of a normalized Abelian differential of the second kind $\nu$ that satisfies*

$$\nu(Q) = dq(k) + \mathcal{O}(k^{-2})dk, \quad k = k(Q) \to \infty, \tag{5.6}$$

$$\oint_{a_l} \nu = 0, \quad \boldsymbol{V}_l = \oint_{b_l} \nu,\ l = 1,\dots,g. \tag{5.7}$$

*Conversely, if two divisors satisfy* (5.5) *then they are the divisors of the poles and zeros of some BA function which satisfies* (5.4).

To determine $\mathbf{\Psi}_p$ we have $D$ and $D'$. We need to show we can choose $\nu = d\kappa + \mathcal{O}(k^{-2})dk$ so that (5.5) holds. The following lemma provides this result.

**Lemma 5.3.** *Assume*

$$D = \sum_{j=1}^{g} Q_j, \quad D' = \sum_{j=1}^{g} R_j, \quad Q_j, R_j \in a_j.$$

*Then there exists real constants* $\{t_j\}_{j=1}^{g}$ *so that the differential*

$$\nu = \sum_{j=1}^{g} t_j \nu_j$$

*satisfies the properties in* (5.6) *with* $q(k) = \kappa(k)$*, and* $\nu_j$ *can be constructed explicitly.*

Proof: *Define* $\tau_j$ *to be the Abelian differential of the second kind with principal part (see Section 2)*

$$\tau_j = (2j-1)\left(k^{2j-3} + \mathcal{O}(k^{-2})\right) dk, \quad k \to \infty,$$

*where* $1/k$ *is a parameter in the neighborhood of* $\infty$*. For* $j \geq 1$*, we choose a path of integration that lies on one sheet. We have*

$$\int_{\lambda_0}^{\lambda} \tau_j = \pm \lambda^{j-1/2}(1 + \mathcal{O}(\lambda^{j-3/2})) \text{ as } \lambda \to \infty.$$

*Define*

$$\nu = \sum_{j=1}^{g} i t_j (\tau_j + \eta_j)$$

*where* $\eta_j$ *is a holomorphic differential chosen so that* $\tau_j + \eta_j$ *has vanishing a periods. We define* $\nu_j = i(\tau_j + \eta_j)$*. Consider the system of equations*

$$\oint_{b_k} \nu = \boldsymbol{V}_k, \quad k = 1, \ldots, g.$$

*It follows that (see Lemma 2.4)*

$$\oint_{b_k} \nu = \sum_{j=1}^{g} i t_j \, \frac{1}{(2j-2)!} \frac{d^{2j-2}}{dz^{2j-2}} r_k(z)\Big|_{z=0}, \quad k = 1, \ldots, g.$$

*Here* $z$ *is a local parameter in the neighborhood of* $\infty$*:* $z(\infty) = 0$ *and* $\omega_k = r_k(z)dz$*. To compute these derivatives we again use a convenient basis, not normalized, for the holomorphic differentials:*

$$u_j = \frac{\lambda^{j-1}}{w} d\lambda, \quad j = 1, \ldots, g.$$

*Set* $\lambda = 1/z^2$ *and compute*

$$\begin{aligned} u_j &= -2z^{2(g-j)} \left( (1 - \alpha_{j+1} z) \prod_{i=1}^{g} (1 - \alpha_i z)(1 - \beta_i z) \right)^{-1/2} dz \\ &= s_j(z) dz. \end{aligned}$$

*It is clear that the matrix*

$$\boldsymbol{A}_{kj} = \frac{d^{2k-2}}{dz^{2k-2}} s_j(z),$$

*is triangular with non-vanishing diagonal entries. There exists an invertible linear transformation from* $\{u_j\}_{j=1}^g$ *to* $\{\omega_k\}_{k=1}^g$*, and since* $\boldsymbol{A}$ *is invertible, it follows that the system*

$$\oint_{b_k} \nu = V_k, \text{ for } k = 1, \ldots, g \tag{5.8}$$

*is uniquely solvable for* $\{t_j\}_{j=1}^g$*. This proves the existence of a BA function with asymptotic behavior* (5.4) *and one arbitrary zero on each a cycle.*

In summary, the BA function $(\Psi_r)_\pm = (\Psi_p)_\pm \Psi_\pm$ has poles located at $(\beta_j, 0)$ and one zero on each $a$-cycle corresponding to the zeros of $\Psi_\pm$. We show below how to compute such a BA function. We use the approach of Section 4 to formulate a RHP for $(\Psi_p)_\pm$:

$$\boldsymbol{\Sigma}_p^+(x,t,\lambda) = \boldsymbol{\Sigma}_p^-(x,t,\lambda) \begin{bmatrix} 0 & 1 \\ 1 & 0 \end{bmatrix}, \ \lambda \in (\alpha_{n+1}, \infty) \cup \bigcup_{j=1}^g (\alpha_j, \beta_j), \tag{5.9}$$

$$\boldsymbol{\Sigma}_p^+(x,t,\lambda) = \boldsymbol{\Sigma}_p^-(x,t,\lambda) \begin{bmatrix} e^{iW_j} & 0 \\ 0 & e^{-iW_j} \end{bmatrix}, \ \lambda \in \bigcup_{j=1}^g (\beta_j, \alpha_{j+1}), \tag{5.10}$$

where each of the $W_j \in \mathbb{R}$ is chosen so that the $g$-function

$$\mathcal{G}_p(\lambda) = \frac{\sqrt{P(\lambda)}}{2\pi i} \sum_{j=1}^g \int_{\beta_j}^{\alpha_{j+1}} \frac{-\kappa(s) + iW_j}{\sqrt{P(\lambda)}^+} \frac{ds}{s-\lambda}, \tag{5.11}$$

satisfies $\mathcal{G}_p(\lambda) = \mathcal{O}(\lambda^{-1/2})$ as $\lambda \to \infty$. Theorem 5.1 provides a well-defined map from $\{t_j\}_{j=1}^g$ to $\{W_j\}_{j=1}^g$. Furthermore each $W_j$ can be taken modulo $2\pi$. The RHP for $(\Psi_r)_\pm$ is similar but $\kappa(\lambda)$ must be replaced with $\kappa(\lambda) + 2ix\lambda^{1/2} + 8it\lambda^{3/2}$ to account for the $x$ and $t$ dependence in $\Psi_\pm$. In this case we write $W_j(x,t)$. This is elaborated below.

# 6 A Riemann–Hilbert problem with smooth solutions

The numerical method described in [20] requires solutions of the RHP to be smooth. We need to deform the RHP to take into account the singularities explicitly if we wish to solve it numerically. In this section, we assume the divisor for the poles of the BA function is

$$D = \sum_{i=1}^g (\beta_j, 0),$$

and that the $\Omega_j(x,t)$ are chosen so that the moment conditions for $\mathcal{G}$ are satisfied. We replace $\Omega_j(x,t)$ with $W_j$ and $W_j(x,t)$ in the case of $(\Psi_p)_\pm$ and $(\Psi_r)_\pm$, respectively. In light of the previous section, all other cases can be reduced to this. Define

$$\boldsymbol{\Delta}(x,t,\lambda) = \begin{bmatrix} \delta(x,t,\lambda) & 0 \\ 0 & 1/\delta(x,t,\lambda) \end{bmatrix}, \quad \delta(x,t,\lambda) = \prod_{j=1}^g \left( \frac{\lambda - \alpha_{j+1}}{\lambda - \beta_j} \right)^{\Omega_j(x,t)/(2\pi)}.$$

The branch cut for $\delta$ to be along the intervals $[\beta_j, \alpha_{j+1}]$ and we assume $\Omega_j(x,t) \in [0, 2\pi)$. Note that $\boldsymbol{\Delta}$ satisfies

$$\boldsymbol{\Delta}^+(x,t,\lambda) = \boldsymbol{\Delta}^-(x,t,\lambda) \begin{bmatrix} e^{i\Omega_j(x,t)} & 0 \\ 0 & e^{-i\Omega_j(x,t)} \end{bmatrix}, \quad \lambda \in (\beta_j, \alpha_{j+1}).$$

Define

$$\boldsymbol{H}(\lambda) = \frac{1}{2} \begin{bmatrix} 1 & 1 + \sqrt{\lambda - \alpha_{n+1}} \\ 1 & 1 - \sqrt{\lambda - \alpha_{n+1}} \end{bmatrix},$$

where the function $\sqrt{\lambda-\alpha_{n+1}}$ has its branch cut on $[\alpha_{n+1},\infty)$, and satisfies $\sqrt{\lambda-\alpha_{n+1}} \sim i|\lambda|^{1/2}$ as $\lambda \to -\infty$ to fix the branch. The last function we need is the $g$-function matrix

$$\boldsymbol{G}(x,t,\lambda) = \begin{bmatrix} e^{-\mathcal{G}(x,t,\lambda)} & 0 \\ 0 & e^{\mathcal{G}(x,t,\lambda)} \end{bmatrix}.$$

Note that if we were solving for $(\Psi_p)_\pm$ or $(\Psi_r)_\pm$ we would replace $\mathcal{G}$ with (5.11).

We introduce a local parametrix for what follows. Consider the RHP

$$Y^+(\lambda) = Y^-(\lambda) \begin{bmatrix} 0 & c \\ 1/c & 0 \end{bmatrix}, \quad \lambda \in (a,b), \tag{6.1}$$

where we do not specify the asymptotic behavior since we wish to obtain multiple solutions. We claim that the function

$$\boldsymbol{Y}(\lambda;a,b,\alpha,\beta,c) = \begin{bmatrix} -i(\lambda-a)^\alpha(\lambda-b)^\beta/c & i(\lambda-a)^\alpha(\lambda-b)^\beta \\ 1/c & 1 \end{bmatrix}, \quad \alpha,\beta = \pm\frac{1}{2},$$

is a solution of (6.1). We choose the branch cut of $(\lambda-a)^\alpha(\lambda-b)^\beta$ to be along the interval $[a,b]$ with $(\lambda-a)^\alpha(\lambda-b)^\beta \sim \lambda^{\alpha+\beta}$ as $\lambda \to \infty$. To simplify notation we define $\boldsymbol{J}_j(x,t) = \operatorname{diag}(e^{-i\Omega_j(x,t)}, e^{i\Omega(x,t)})$ and

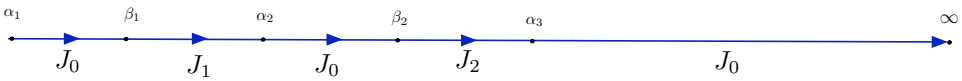


Figure 3: The contours and jump matrices of the RHP for $\boldsymbol{\Sigma}$.

$$\boldsymbol{J}_0 = \begin{bmatrix} 0 & 1 \\ 1 & 0 \end{bmatrix}.$$

We need a local parametrix at each point $\alpha_j$ or $\beta_j$. This motivates the definition

$$\begin{aligned}
&\boldsymbol{A}_1(x,t,\lambda) = \boldsymbol{Y}(\lambda;\alpha_1,\beta_1,1/2,-1/2,1),\\
&\boldsymbol{A}_j(x,t,\lambda) = \boldsymbol{Y}(\lambda;\alpha_j,\beta_j,1/2,-1/2,\exp(-i\Omega_{j-1}(x,t))), \quad j=2,\dots,g+1,\\
&\boldsymbol{B}_j(x,t,\lambda) = \boldsymbol{Y}(\lambda;\alpha_j,\beta_j,1/2,-1/2,\exp(-i\Omega_j(x,t))), \quad j=1,\dots,g.
\end{aligned}$$

This allows us to enforce boundedness at each $\alpha_j$ with a possibly unbounded singularity at $\beta_j$. The matrices $\boldsymbol{A}_j$ are used locally at $\alpha_j$ and $\boldsymbol{B}_j$ at $\beta_j$.

Consider the following example. The general case can be inferred from this.

**Example 6.1** (Genus two)**.** *Our initial RHP is* (5.2) *with the condition*

$$\lim_{\lambda\to\infty} \boldsymbol{\Sigma}(x,t,\lambda) = \begin{bmatrix} 1 & 1 \end{bmatrix},$$

*see Figure 3. First, we introduce a circle around $\alpha_3 = \alpha_{g+1}$. In addition we place a large circle around all the gaps, see Figure 4. Now, we redefine our function $\boldsymbol{\Sigma}$ in various regions. Define $\boldsymbol{\Sigma}_1$ by the piecewise definition in Figure 5(a). We compute the jumps satisfied by $\boldsymbol{\Sigma}_1$, see Figure 5(b). An important calculation is that if $\boldsymbol{\Sigma}_1(x,t,\lambda) = \begin{bmatrix} 1 & 1 \end{bmatrix} + \mathcal{O}(\lambda^{-1})$ then*

$$\begin{aligned}
\boldsymbol{\Sigma}_1(x,t,\lambda)\boldsymbol{H}(\lambda) &= \frac{1}{2}\left(\begin{bmatrix} 1 & 1 \end{bmatrix} + \mathcal{O}(\lambda^{-1})\right) \begin{bmatrix} 1 & 1+\sqrt{\lambda-\alpha_{n+1}} \\ 1 & 1-\sqrt{\lambda-\alpha_{n+1}} \end{bmatrix}\\
&= \begin{bmatrix} 1 & 1 \end{bmatrix} + \mathcal{O}(\lambda^{-1/2}).
\end{aligned}$$

*This allows us to obtain functions with the correct asymptotic behavior.*

*We present the deformation in the interior of the large circle in Figure 5(a). See Figure 6(a) for the piecewise definition of $\mathbf{\Sigma}_2$ and Figure 6(b) for the jumps and jump contours for $\mathbf{\Sigma}_2$. While this RHP can be solved numerically, we make a final deformation to reduce the number of contours present. Define $\mathcal{D}$ to be the region inside the large outer circle but outside each of the smaller circles around $\alpha_j, \beta_j$. Then define*

$$\mathbf{\Sigma}_3(x,t,\lambda) = \begin{cases} \mathbf{\Sigma}_2(x,t,\lambda)\mathbf{\Delta}^{-1}(x,t,\lambda) & \text{if } \lambda \in \mathcal{D}, \\ \mathbf{\Sigma}_2(x,t,\lambda) & \text{otherwise.} \end{cases}$$

*See Figure 7 for the jumps and jump contours of the RHP for $\mathbf{\Sigma}_3$. We refer to this as the deformed and regularized RHP associated with $\Psi_\pm$.*

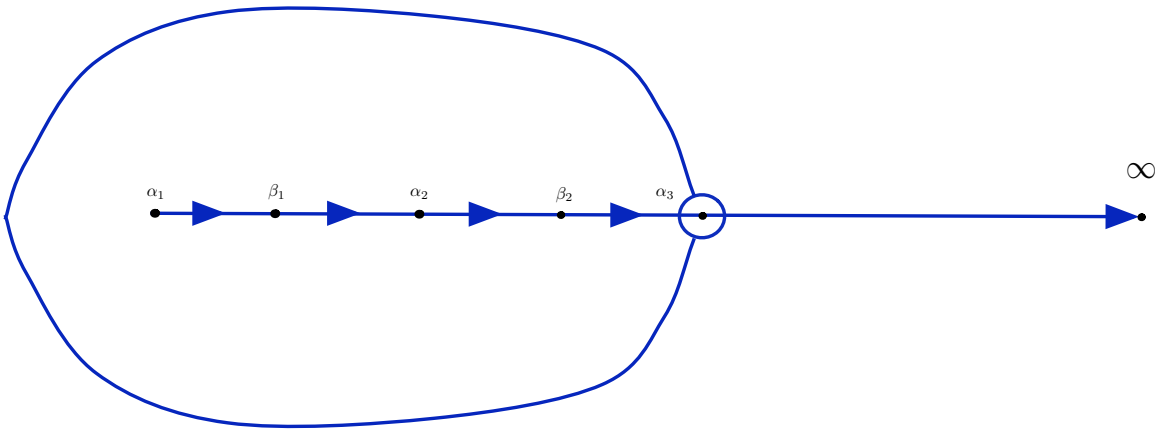


Figure 4: Introducing a large circle around $\alpha_j$ and $\beta_j$.

*This resulting RHP has smooth solutions by the theory of [25]. Furthermore, the uniqueness of the BA function gives us existence and uniqueness of the solution of this RHP. See Appendix A for a more detailed discussion of the solvability of the RHP. This justifies solving for $\mathbf{\Sigma}_3$ numerically.*

## 6.1 Reconstruction of the solution to the KdV equation

Once the function $\mathbf{\Sigma}_3$ above is known (at least numerically) we want to extract from it the solution of the KdV equation. We use that $\mathbf{\Sigma}_3$ is analytic at infinity and that each component of $\mathbf{\Psi}$ satisfies (3.1). For $\lambda$ large we write

$$\mathbf{\Sigma}_3(x,t,\lambda) = \mathbf{\Psi}(x,t,\lambda)\boldsymbol{R}(x,t,\lambda)\boldsymbol{G}(x,t,\lambda)\boldsymbol{H}(\lambda). \tag{6.2}$$

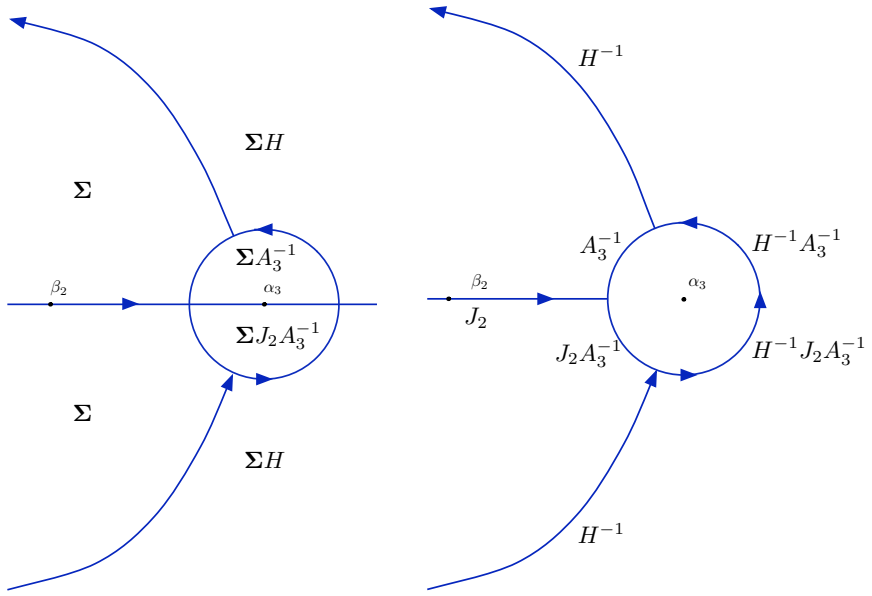


(a) (b)

Figure 5: (a) The piecewise definition of $\mathbf{\Sigma}_1$. (b) The jump contours and jump matrices for the RHP for $\mathbf{\Sigma}_1$.

We find a differential equation for $\mathbf{\Sigma}_3$. Differentiating (6.2) we find

$$\begin{aligned}
\partial_x\mathbf{\Sigma}_3(x,t,\lambda) = \partial_x\mathbf{\Psi}(x,t,\lambda)\boldsymbol{R}(x,t,\lambda)\boldsymbol{G}(x,t,\lambda)\boldsymbol{H}(\lambda)+\\
\mathbf{\Psi}(x,t,\lambda)\partial_x\boldsymbol{R}(x,t,\lambda)\boldsymbol{G}(x,t,\lambda)\boldsymbol{H}(\lambda)+\\
\mathbf{\Psi}(x,t,\lambda)\boldsymbol{R}(x,t,\lambda)\partial_x\boldsymbol{G}(x,t,\lambda)\boldsymbol{H}(\lambda).\\
\partial_{xx}\mathbf{\Sigma}_3(x,t,\lambda) = \partial_{xx}\mathbf{\Psi}(x,t,\lambda)\boldsymbol{R}(x,t,\lambda)\boldsymbol{G}(x,t,\lambda)\boldsymbol{H}(\lambda)+\\
\partial_x\mathbf{\Psi}(x,t,\lambda)\partial_x\boldsymbol{R}(x,t,\lambda)\boldsymbol{G}(x,t,\lambda)\boldsymbol{H}(\lambda)+\\
\partial_x\mathbf{\Psi}(x,t,\lambda)\boldsymbol{R}(x,t,\lambda)\boldsymbol{\partial}_xG(x,t,\lambda)\boldsymbol{H}(\lambda)+\\
\partial_x\mathbf{\Psi}(x,t,\lambda)\partial_x\boldsymbol{R}(x,t,\lambda)\boldsymbol{G}(x,t,\lambda)\boldsymbol{H}(\lambda)+\\
\mathbf{\Psi}(x,t,\lambda)\partial_{xx}\boldsymbol{R}(x,t,\lambda)\boldsymbol{G}(x,t,\lambda)\boldsymbol{H}(\lambda)+\\
\mathbf{\Psi}(x,t,\lambda)\partial_x\boldsymbol{R}(x,t,\lambda)\partial_x\boldsymbol{G}(x,t,\lambda)\boldsymbol{H}(\lambda)+\\
\partial_x\mathbf{\Psi}(x,t,\lambda)\boldsymbol{R}(x,t,\lambda)\partial_x\boldsymbol{G}(x,t,\lambda)\boldsymbol{H}(\lambda)+\\
\mathbf{\Psi}(x,t,\lambda)\partial_x\boldsymbol{R}(x,t,\lambda)\partial_x\boldsymbol{G}(x,t,\lambda)\boldsymbol{H}(\lambda)+\\
\mathbf{\Psi}(x,t,\lambda)\boldsymbol{R}(x,t,\lambda)\partial_{xx}\boldsymbol{G}(x,t,\lambda)\boldsymbol{H}(\lambda).
\end{aligned}$$

We seek to simplify this formula. Define $\boldsymbol{r}(\lambda) = \operatorname{diag}(2i\lambda^{1/2}, -2i\lambda^{1/2})$ then

$$\begin{aligned}
\partial_x\boldsymbol{R}(x,t,\lambda) &= \boldsymbol{r}(\lambda)\boldsymbol{R}(x,t,\lambda),\\
\partial_{xx}\boldsymbol{R}(x,t,\lambda) &= \boldsymbol{r}^2(\lambda)\boldsymbol{R}(x,t,\lambda).
\end{aligned}$$

It follows that each $\Omega_j(x,t)$ depends linearly on $x$. Define $\boldsymbol{g}(\lambda) = \operatorname{diag}(-\partial_x g(x,t,\lambda), \partial_x g(x,t,\lambda))$, therefore

$$\begin{aligned}
\partial_x\boldsymbol{G}(x,t,\lambda) &= \boldsymbol{g}(\lambda)\boldsymbol{G}(x,t,\lambda),\\
\partial_{xx}\boldsymbol{G}(x,t,\lambda) &= \boldsymbol{g}^2(\lambda)\boldsymbol{G}(x,t,\lambda).
\end{aligned}$$

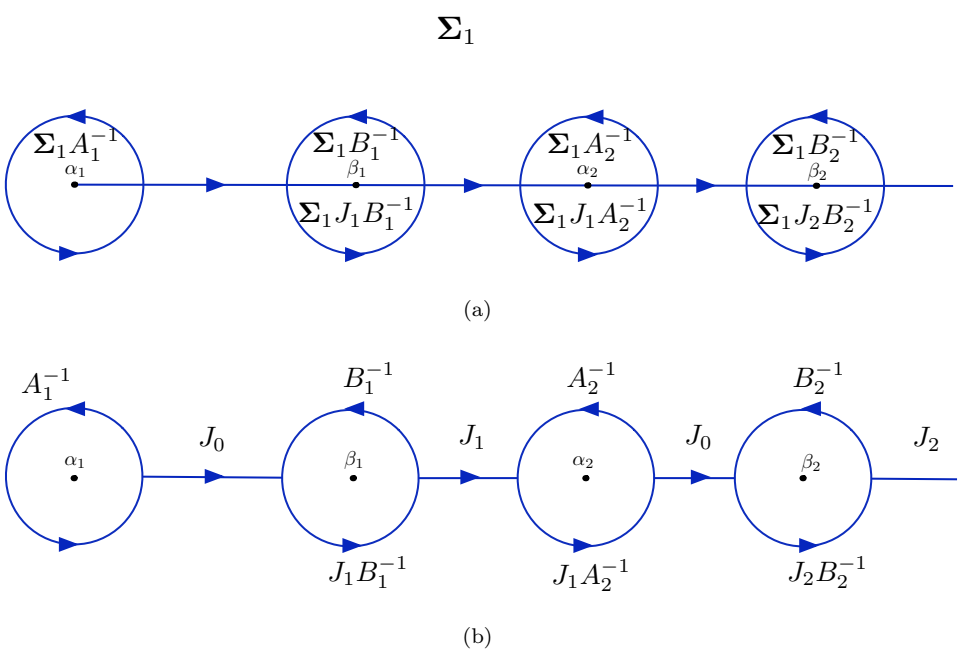


Figure 6: (a) The piecewise definition of $\boldsymbol{\Sigma}_2$ inside the outer circle. (b) The jump contours and jump matrices for the RHP for $\boldsymbol{\Sigma}_2$.

Also, $\boldsymbol{R}, \boldsymbol{G}, \boldsymbol{r}$ and $\boldsymbol{g}$ are diagonal and mutually commute. We write

$$\begin{aligned}
\partial_x \boldsymbol{\Sigma}_3(x,t,\lambda) &= \partial_x \boldsymbol{\Psi}(x,t,\lambda)\boldsymbol{R}(x,t,\lambda)\boldsymbol{G}(x,t,\lambda)\boldsymbol{H}(\lambda) \\
&\quad + \boldsymbol{\Psi}(x,t,\lambda)\boldsymbol{R}(x,t,\lambda)\boldsymbol{G}(x,t,\lambda)\boldsymbol{H}(\lambda)\boldsymbol{H}^{-1}(\lambda)[\boldsymbol{r}(\lambda)+\boldsymbol{g}(\lambda)]\boldsymbol{H}(\lambda), \\
\partial_{xx} \boldsymbol{\Sigma}_3(x,t,\lambda) &= \partial_{xx} \boldsymbol{\Psi}(x,t,\lambda)\boldsymbol{R}(x,t,\lambda)\boldsymbol{G}(x,t,\lambda)\boldsymbol{H}(\lambda) \\
&\quad + 2\partial_x \boldsymbol{\Psi}(x,t,\lambda)\boldsymbol{R}(x,t,\lambda)\boldsymbol{G}(x,t,\lambda)\boldsymbol{H}(\lambda)\boldsymbol{H}^{-1}(\lambda)[\boldsymbol{r}(\lambda)+\boldsymbol{g}(\lambda)]\boldsymbol{H}(\lambda) \\
&\quad + \boldsymbol{\Psi}(x,t,\lambda)\boldsymbol{R}(x,t,\lambda)\boldsymbol{G}(x,t,\lambda)\boldsymbol{H}(\lambda)\boldsymbol{H}^{-1}(\lambda)[\boldsymbol{g}^2(\lambda)+2\boldsymbol{g}(\lambda)\boldsymbol{r}(\lambda)+\boldsymbol{r}^2(\lambda)]\boldsymbol{H}(\lambda).
\end{aligned}$$

We proceed to eliminate $\boldsymbol{\Psi}$. Since $\partial_{xx}\boldsymbol{\Psi} = -\lambda\boldsymbol{\Psi} - u(x,t)\boldsymbol{\Psi}$, we obtain

$$\begin{aligned}
\partial_{xx} \boldsymbol{\Sigma}_3(x,t,\lambda) &= [-\lambda - u(x,t)]\boldsymbol{\Sigma}_3(x,t,\lambda) + 2\partial_x \boldsymbol{\Sigma}_3(x,t,\lambda)\boldsymbol{H}^{-1}(\lambda)[\boldsymbol{g}(\lambda)+\boldsymbol{r}(\lambda)]\boldsymbol{H}(\lambda) \\
&\quad - \boldsymbol{\Sigma}_3(x,t,\lambda)\boldsymbol{H}^{-1}(\lambda)[\boldsymbol{g}(\lambda)+\boldsymbol{r}(\lambda)]^2\boldsymbol{H}(\lambda).
\end{aligned} \tag{6.3}$$

Set $\boldsymbol{\Sigma}_3(x,t,\lambda) = \begin{bmatrix} 1 & 1 \end{bmatrix} + \boldsymbol{c}_1(x,t)/\lambda + \mathcal{O}(\lambda^{-2})$ and substitute, assuming each derivative of $\boldsymbol{\Sigma}_3$ has an induced asymptotic expansion,

$$\begin{aligned}
\partial_{xx}\boldsymbol{c}_1(x,t)/\lambda + \mathcal{O}(\lambda^{-2}) &= [-\lambda - u(x,t)](\begin{bmatrix} 1 & 1 \end{bmatrix} + \boldsymbol{c}_1(x,t)/\lambda + \mathcal{O}(\lambda^{-2})) \\
&\quad + (\begin{bmatrix} 1 & 1 \end{bmatrix} + \partial_x\boldsymbol{c}_1(x,t)/\lambda + \mathcal{O}(\lambda^{-2}))\boldsymbol{H}^{-1}(\lambda)[\boldsymbol{g}(\lambda)+\boldsymbol{r}(\lambda)]\boldsymbol{H}(\lambda) \\
&\quad + (\begin{bmatrix} 1 & 1 \end{bmatrix} + \boldsymbol{c}_1(x,t)/\lambda + \mathcal{O}(\lambda^{-2}))\boldsymbol{H}^{-1}(\lambda)[\boldsymbol{g}(\lambda)+\boldsymbol{r}(\lambda)]^2\boldsymbol{H}(\lambda).
\end{aligned}$$

It can be shown that the $\mathcal{O}(\lambda)$ terms on each side of this equation cancel. Equating the $\mathcal{O}(1)$ terms we obtain

$$\begin{aligned}
u(x,t)\begin{bmatrix} 1 & 1 \end{bmatrix} &= -\lim_{\lambda\to\infty} \partial_x\boldsymbol{c}_1(x,t)/\lambda\boldsymbol{H}^{-1}(\lambda)[\boldsymbol{g}(\lambda)+\boldsymbol{r}(\lambda)]\boldsymbol{H}(\lambda) \\
&\quad - \lim_{\lambda\to\infty}\left(\begin{bmatrix} -\lambda & -\lambda \end{bmatrix} + (\begin{bmatrix} 1 & 1 \end{bmatrix} + \boldsymbol{c}_1(x,t)/\lambda + \mathcal{O}(\lambda^{-2}))\boldsymbol{H}^{-1}(\lambda)[\boldsymbol{g}(\lambda)+\boldsymbol{r}(\lambda)]^2\boldsymbol{H}(\lambda)\right).
\end{aligned}$$

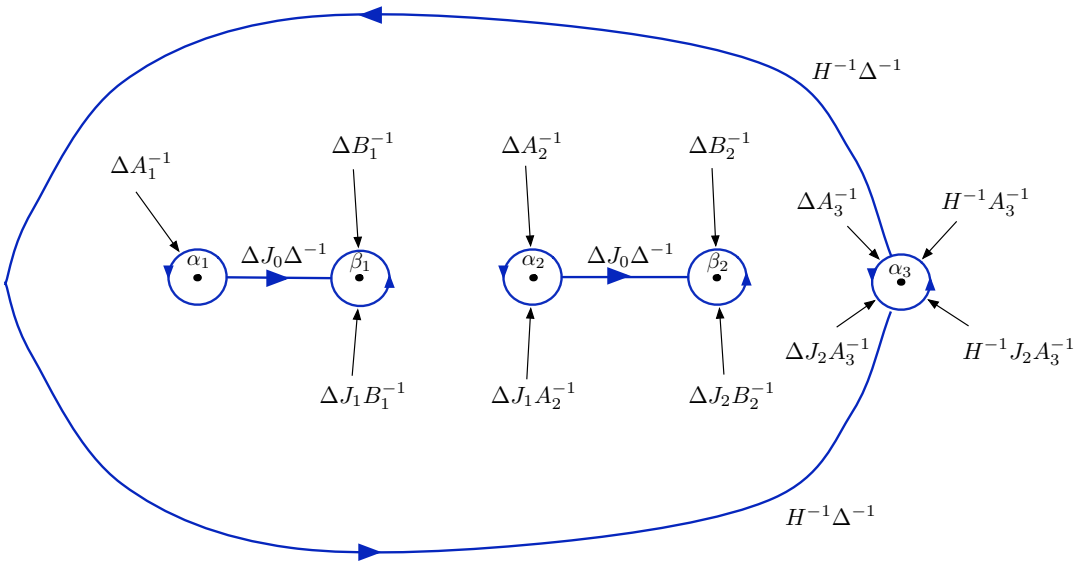


Figure 7: The final RHP for $\mathbf{\Sigma}_3$. The same deformation works for RHPs which arise from arbitrary genus BA functions by adding additional contours.

Equating $\partial_x \boldsymbol{c}_1(x,t) = \begin{bmatrix} s_1(x,t) & s_2(x,t) \end{bmatrix}$ and working this out explicitly, we find

$$u(x,t) = 2i(s_2(x,t) - s_1(x,t)) + 2iE, \tag{6.4}$$
$$E = -\frac{1}{2\pi}\sum_{n=1}^{g}\int_{\beta_n}^{\alpha_{n+1}} \frac{\partial_x \Omega_n(x,t) - 2\lambda^{1/2}}{\sqrt{P(\lambda)}^{+}}\lambda^g d\lambda.$$

## 6.2 Regularization of the RHP with poles in the gaps

In this section we deal with the case where the divisor for the poles of the BA function is of the form

$$D = \sum_{i=1}^{g} Q_i, \quad Q_i \in a_i.$$

We have proved existence of a BA function with one arbitrary zero on each $a$-cycle. We consider the BA function $(\Psi_r)_\pm = (\Psi_p)_\pm \Psi_\pm$ which has poles located at $\{(0,\beta_j)\}_{j=1}^g$ and one zero on each $a$-cycle. In this section we assume we know $t_1, t_2, \ldots$ which are required to find $(\Psi_p)_\pm$. In the next section we discuss computing $\{t_j\}_{j=1}^g$. It follows that

$$(\Psi_r)_\pm \sim e^{\pm Z(x,t,\lambda)/2}, \tag{6.5}$$

where

$$Z(x,t,\lambda) = \kappa(\lambda) + 2ix\lambda^{1/2} + 8it\lambda^{3/2} = 2i(x+t_1)\lambda^{1/2} + 2i(4t+t_2)\lambda^{3/2} + 2i\sum_{j=3}^{g} t_j \lambda^{(2j-1)/2}.$$

Using the techniques in Section 6.1 we see this is all the information that is needed to set up a solvable RHP for $(\Psi_r)_\pm$ with smooth solutions.

We have to extract the solution to the KdV equation from $(\Psi_r)_\pm$. We solve for a function $\mathbf{\Sigma}_3$, the deformation of $\mathbf{\Psi}_r$, that satisfies

$$\begin{aligned}\mathbf{\Sigma}_3(x,t,\lambda) &= \mathbf{\Psi}(x,t,\lambda)\boldsymbol{R}(x,t,\lambda)\boldsymbol{G}(x,t,\lambda)\mathbf{\Psi}_p'(\lambda)\boldsymbol{H}(\lambda),\\ \mathbf{\Psi}_p'(\lambda) &= \operatorname{diag}\mathbf{\Psi}_p(\lambda),\end{aligned} \tag{6.6}$$

for large $\lambda$. If we perform the same calculations which results in (6.3). We obtain

$$\begin{aligned}\partial_{xx}\mathbf{\Sigma}_3(x,t,\lambda) = [-\lambda - u(x,t)]\mathbf{\Sigma}_3(x,t,\lambda) + 2\partial_x\mathbf{\Sigma}_3(x,t,\lambda)\boldsymbol{H}^{-1}(\lambda)(\mathbf{\Psi}_p'(\lambda))^{-1}[\boldsymbol{g}(\lambda)+\boldsymbol{r}(\lambda)]\mathbf{\Psi}_p'(\lambda)\boldsymbol{H}(\lambda)\\ -\mathbf{\Sigma}_3(x,t,\lambda)\boldsymbol{H}^{-1}(\lambda)(\mathbf{\Psi}_p'(\lambda))^{-1}[\boldsymbol{g}(\lambda)+\boldsymbol{r}(\lambda)]^2\mathbf{\Psi}_p'(\lambda)\boldsymbol{H}(\lambda).\end{aligned} \tag{6.7}$$

But $\mathbf{\Psi}_p'$ is diagonal and commutes with $\boldsymbol{g}$ and $\boldsymbol{h}$. Therefore, all $\mathbf{\Psi}_p'$ dependence cancels out. We see that (6.4) is invariant under multiplication by $(\Psi_p)_\pm$. Thus, the solution $u(x,t)$ to the KdV equation is extracted from $\mathbf{\Sigma}_3$ by (6.4). We summarize our results in the following theorem.

**Theorem 6.1.** *If $\mathbf{\Sigma}_3(x,t,\lambda)$ is the solution of the deformed and regularized RHP associated with $(\Psi_r)_\pm$ and*

$$\mathbf{\Sigma}_3(x,t,\lambda) = \begin{bmatrix} 1 & 1 \end{bmatrix} + \boldsymbol{c}_1(x,t)\lambda^{-1} + \mathcal{O}(\lambda^{-2}), \quad \boldsymbol{c}_1(x,t) = \begin{bmatrix} s_1(x,t) & s_2(x,t) \end{bmatrix},$$

*then the corresponding solution of the KdV equation is found through*

$$\begin{aligned}u(x,t) &= 2i(s_2(x,t) - s_1(x,t) + 2iE,\\ E &= -\frac{1}{2\pi}\sum_{j=1}^{g}\int_{\beta_j}^{\alpha_{j+1}} \frac{\partial_x W_j(x,t) - 2\lambda^{1/2}}{\sqrt{P(\lambda)}^+}\lambda^g d\lambda,\end{aligned}$$

*where $\{W_j(x,t)\}_{j=1}^\infty$ are defined by the moment conditions for (5.11) with $\kappa(\lambda)$ replaced with $Z(x,t,\lambda)$.*

This theorem states that despite the theoretical use of the function $(\Psi_p)_\pm$, the computation of the solution to the KdV equation does not require the computation of $(\Psi_p)_\pm$.

# 7 Numerical computation

In this section we discuss the computation of all the components of the theory. These components are:

1. Evaluating contour integrals used in the Abel map and the moment problem.
2. Computing the singular integrals used in the representation of the $g$-function.
3. Solving the deformed and regularized RHP for the Baker–Akhiezer function.
4. Extracting the solution to the KdV equation from the Baker–Akhiezer function.

## 7.1 Computing contour integrals

The developments above require the computation of integrals of the form

$$I_j(f) = \int_{\beta_j}^{\alpha_{j+1}} \frac{f(\lambda)}{\sqrt{P(\lambda)}^+}d\lambda, \tag{7.1}$$

to determine the $g$-function and compute $\Omega_j/W_j$. Note that in the cases we consider $f$ is analytic near the contour of integration. Also, we compute the Abel map of divisors whose points lie in gaps. We always choose $Q_0 = (\alpha_1, 0)$ in (2.1) and integrate along $\Gamma_+$ across the bands and gaps. Thus computing the Abel map of a point in a gap requires computation of integrals of the form (7.1) along with integrals of the form

$$\begin{aligned}K_j(f) &= \int_{\alpha_j}^{\beta_j} \frac{f(\lambda)}{\sqrt{P(\lambda)}^+}d\lambda,\\ I_j(f,\lambda) &= \int_{\beta_j}^{\lambda} \frac{f(s)}{\sqrt{P(s)}^+}ds.\end{aligned} \tag{7.2}$$

While numerical integration packages can handle such integrals, it is beneficial to use Chebyshev polynomials. For example, define

$$s = m(\lambda) = \frac{2}{\beta_j - \alpha_j}\lambda - \frac{\beta_j + \alpha_j}{\beta_j - \alpha_j}.$$

We change (7.1) to

$$I_j(f) = \int_{-1}^{1} \frac{f(m^{-1}(s))}{\sqrt{P(m^{-1}(s))}^+} dm^{-1}(s).$$

The function

$$w(s) = \frac{\sqrt{1-s^2}}{\sqrt{P(m^{-1}(s))}},$$

is analytic in a neighborhood of the interval $[-1, 1]$. We write

$$I_j(f) = \int_{-1}^{1} \left( \frac{f(m^{-1}(s))}{\sqrt{P(m^{-1}(s))}^+} w(s) \frac{d}{ds} m^{-1}(s) \right) \frac{ds}{\sqrt{1-s^2}}.$$

The Chebyshev series approximation of the function in parenthesis converge exponentially since it is analytic in a neighborhood of $[-1, 1]$. A discrete cosine transform is used to approximate the series and the first coefficient in the series gives a very good approximation to $I_j(f)$. Similar ideas work for $K_j(f)$ but we must modify our approach for $I_j(f, \lambda)$. Consider the integral

$$F_n(\lambda) = \int_{-1}^{\lambda} T_n(x) \frac{dx}{\sqrt{1-x^2}}, \quad \lambda \in (1, 1).$$

Here $T_n$ denotes the $n$th-order Chebyshev polynomial of the second kind. Using the standard change of variables $x = \cos\theta$,

$$F_n(\lambda) = -\int_{\pi}^{\arccos\lambda} T_n(\cos\theta) d\theta = -\int_{\pi}^{\arccos\lambda} \cos(n\theta) d\theta.$$

Therefore

$$F_n(\lambda) = \begin{cases} -\frac{\sin(n \arccos\lambda)}{n} & \text{if } n > 0, \\ \pi - \arccos\lambda & \text{if } n = 0. \end{cases}$$

Using the change of variables $m(\lambda)$ and the discrete cosine transform we can compute each $I_j(f, \lambda)$ with this formula.

Weneed to compute $b$ periods. The $b$ cycles have a more complicated relationship. Consider the cycles $\tilde{b}_j$ in Figure 8. We compute

$$\oint_{\tilde{b}_j} w = 2 \int_{\alpha_j}^{\beta_j} f(\lambda) d\lambda.$$

From Figure 8, we see that $b_1 = \tilde{b}_1$ and $b_i = \tilde{b}_i + b_{i-1}$. This gives a recursion relationship for $b$ cycles.

We must know $\omega_k$ before computing the Abel map. We describe how to compute the normalized differentials. Let $\omega = f(\lambda)d\lambda$ be a holomorphic differential, we showed in the proof of Theorem 5.1 that

$$\oint_{a_j} w = -2 \int_{\beta_j}^{\alpha_{j+1}} f(\lambda) d\lambda.$$

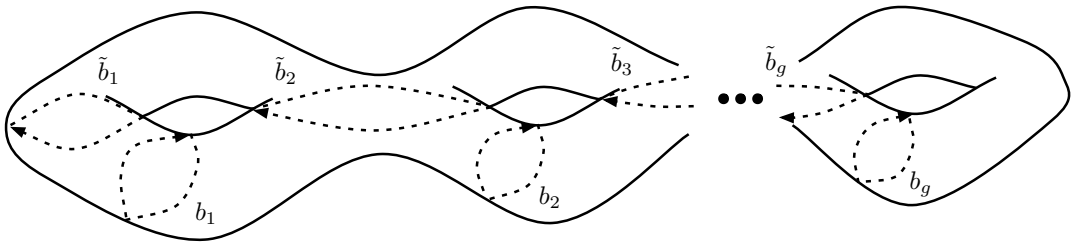


Figure 8: The cycles $\tilde{b}_j$ on a schematic of the Riemann surface.

Given the branch point $\alpha_j, \beta_j$, $j = 1, \ldots, g+1$ where $\beta_{g+1} = \infty$ we use the basis of unnormalized differentials

$$u_n = \frac{\lambda^{n-1}}{\mu} d\lambda, \quad n = 1, \ldots, g,$$

and compute their $a$ and $b$-periods. This allows us to construct the basis $\omega_k$ of normalized differentials and gives us access to the Abel map.

Assume $Q = (\lambda, \sigma\sqrt{P(\lambda)}^{+}) \in a_j$ for $\sigma = \pm 1$. Then the $k$th component of the Abel map is computed by

$$(A(Q))_k = \sum_{l=1}^{j-1} (I_l(f_k) + K_l(f_k)) + K_l(f_k) + \sigma I_j(f_k, \lambda),$$

where $f_k(\lambda)/w$ is the principal part of $\omega_k$, the $k$th normalized holomorphic differential.

## 7.2 Computing the $g$-function

The $g$-function is defined by

$$\mathcal{G}(x,t,\lambda) = \frac{\sqrt{P(\lambda)}}{2\pi i} \sum_{j=1}^{g} \int_{\beta_j}^{\alpha_{j+1}} \frac{-\zeta(x,t,s) + i\Omega_j(x,t)}{\sqrt{P(s)}^{+}} \frac{ds}{s-\lambda}, \tag{7.3}$$

see (5.1). After mapping each interval of integration in (7.3) using a linear change of variables $z = m_j(s)$ ($m_j : [\beta_j, \alpha_{j+1}] \to [-1, 1]$) we have the expression

$$\mathcal{G}(x,t,\lambda) = \frac{\sqrt{P(\lambda)}}{2\pi i} \sum_{j=1}^{g} \int_{-1}^{1} H_j(z) \frac{dz}{z - m_j(\lambda)},$$

where

$$H_j(z) = \frac{-\zeta(x,t,m_j^{-1}(z)) + i\Omega_j(x,t)}{\sqrt{P(m_j^{-1}(z))}^{+}}.$$

Note that $F_j(z) = H_j(z)\sqrt{1-z^2}$ is analytic in a neighborhood of $[-1, 1]$. We use

$$\mathcal{G}(x,t,\lambda) = \frac{\sqrt{P(\lambda)}}{2\pi i} \sum_{j=1}^{g} \int_{-1}^{1} \frac{F_j(z)}{z - m_j(\lambda)} \frac{dz}{\sqrt{1-z^2}},$$

This reduces the problem of computing the $g$-function to that of computing integrals of the form

$$C(\lambda) = \frac{1}{2\pi i} \int_{-1}^{1} \frac{f(s)}{(s-\lambda)} \frac{1}{\sqrt{1-s^2}} ds, \quad \lambda \notin [-1, 1],$$

where $f$ is a smooth function on $[-1,1]$. We use the known expansion of the function $1/(s-\lambda)$ in a Chebyshev series [23]

$$\frac{1}{s-\lambda}=\sum_{j=0}^{\infty}e_j(\lambda)T_j(s),\quad e_j(\lambda)=\begin{cases}-\frac{1}{\sqrt{\lambda^2-1}} & \text{if } j=0,\\ -2\frac{(\lambda-\sqrt{\lambda^2-1})^j}{\sqrt{\lambda^2-1}} & \text{otherwise.}\end{cases}$$

Here $T_j$ is the $j$th Chebyshev polynomial of the second kind [23]. This formula is technically valid for $\lambda>1$ but can be extended to $\mathbb{C}\setminus[-1,1]$ by analytic continuation. We use a discrete cosine transformation of order $n$ to approximate the Chebyshev series of $f$:

$$f(s)\approx\sum_{j=0}^{n}c_jT_j(s).$$

Orthogonality gives

$$C(\lambda)\approx\frac{1}{2\pi i}\left(\pi c_0e_0(\lambda)+\frac{\pi}{2}\sum_{j=0}^{n}c_je_j(\lambda)\right).$$

Exponential convergence is guaranteed since in our case $f$ is analytic.

Alhough it is not important for our purposes, one may wish to compute the limiting values $\mathcal{G}^{\pm}$ as $\lambda$ approaches a gap from above or below. We use the formula [19]

$$\lim_{\epsilon\to0^+}\frac{1}{2\pi i}\int_{-1}^{1}\frac{T_j(s)}{s-(\lambda\pm i\epsilon)}\frac{ds}{\sqrt{1-s^2}}=\frac{1}{2}T_j(\lambda)\pm\frac{1}{2i}U_{j-1}(\lambda),\quad\lambda\in(-1,1),$$

where $U_k$ is the Chebyshev polynomial of the first kind [23].

## 7.3 Computing the Baker-Akhiezer function

This section is concerned with computing $(\Psi_r)_{\pm}$. Let $D'$ be the divisor for the desired zeros of the BA function and $D$ be the divisor for the poles. We compute the vector (see (5.5))

$$\boldsymbol{V}=A(D'-D),$$

using the method for computing integrals described above. Next, consider the differentials

$$\nu_j=i\frac{\lambda^{g+j-1}}{\mu}d\lambda,\quad j=1,\dots,g,$$

which satisfy

$$\int_{\lambda_0}^{\lambda}\nu_j=\mathcal{O}(\lambda^{-1/2+j}),\text{ as }\lambda\to\infty.$$

We accurately compute the $a$-periods of $\nu_j$. We construct $\{\tilde{\nu}_j\}_{j=1}^{g}$ which each have vanishing $a$ periods by adding an appropriate linear combination holomorphic differentials. We compute the matrix

$$\boldsymbol{S}_{kj}=\oint_{b_k}\tilde{\nu}_j.$$

The system $\boldsymbol{SX}=\boldsymbol{V}$ is solved for the real-valued vector $\boldsymbol{X}$, giving a differential

$$l=\sum_{j=1}^{g}\boldsymbol{X}_j\tilde{x}_j,$$

that has $b$ periods equal to the vector $\boldsymbol{V}$. The final step is to compute the coefficients $\{t_j\}_{j=1}^{g}$ in the expansion

$$\int_{\lambda_0}^{\lambda} l = \sum_{n=1}^{g} i t_n \lambda^{n-1/2} + \mathcal{O}(\lambda^{-1/2}) = \kappa(\lambda)/2 + \mathcal{O}(\lambda^{-1/2}).$$

The BA function with asymptotic behavior $(\Psi_p)_\pm \sim e^{\pm\kappa(\lambda)/2}$ as $\lambda \to \infty$ has zeros at the points of $D'$. Theorem 6.1 tells us to seek $(\Psi_r)_\pm \sim e^{\pm Z(x,t,\lambda)/2}$ as $\lambda \to \infty$. We construct the deformed and regularized RHP for $(\Psi_r)_\pm$, see Section 6. This RHP is solved numerically.

To test the method we use $\alpha_1 = 0, \beta_1 = .25, \alpha_2 = 1, \beta_2 = 1.5$ and $\alpha_3 = 2$. Thus we have a genus two surface. We choose zeros to be at the points $(.5, \sqrt{P(.5)}^{+})$ and $(1.75, \sqrt{P(1.75)}^{+})$. To approximate the BA function we use $n$ collocation points per contour. See Appendix B for a more thorough discussion of the numerical method for RHPs that is used and its convergence properties. The roots of the approximate BA function are found using standard Chebyshev root-finding techniques [3]. In Figure 9 we plot the absolute error of the roots as $n$ increases. Spectral convergence of the roots is observed. See Figure 10 for a surface plot showing both the zeros and the poles of the BA function on a single sheet. See Figures 11 and 12 for contour plots of the real part, imaginary part, and modulus of the BA function on each sheet. Note that producing this plot requires the computation of the $g$-function. These plots are all produced in the genus two case but higher genus BA functions can also be plotted.

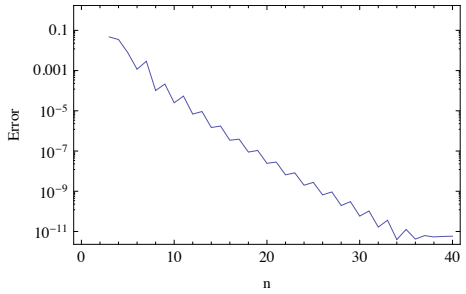


Figure 9: A demonstration of the spectral convergence of the zeros of the BA function.

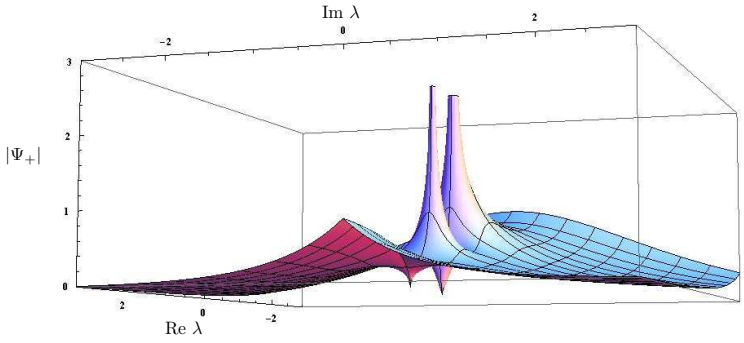


Figure 10: A three-dimensional plot of the modulus of the BA function on one sheet of the Riemann surface. We see two poles and two zeros are clearly present.

## 7.4 Numerical solutions of the KdV equation

Before we move to numerical results for the KdV equation, let us review the solution process. The constants $\alpha_j$ $(j = 1, \ldots, g+1)$ and $\beta_j$ $(j = 1, \ldots, g)$ are chosen, all positive. This determines the polynomial $P(\lambda)$

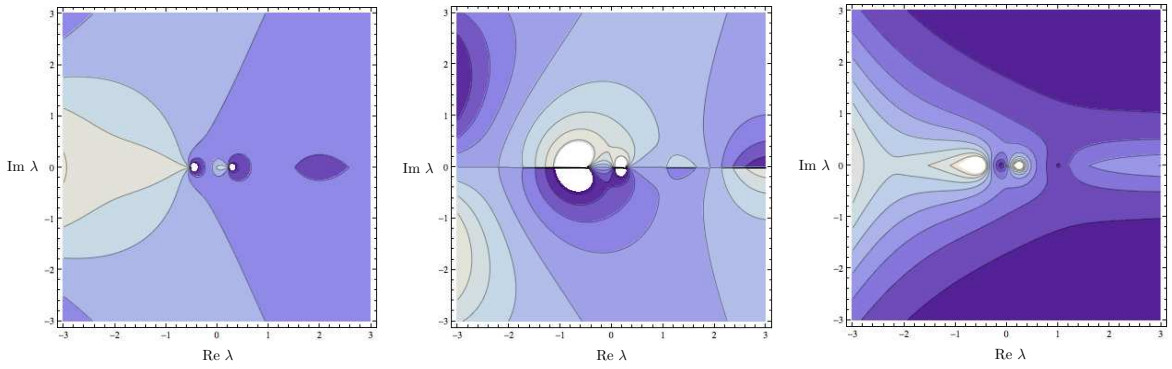


Figure 11: A genus-two Baker–Akhiezer function. Darker shades indicate smaller values. Two poles and two zeros are clearly present. (a) The real part of $\Psi_+$. (b) The imaginary part of $\Psi_+$. (c) The modulus of $\Psi_+$.

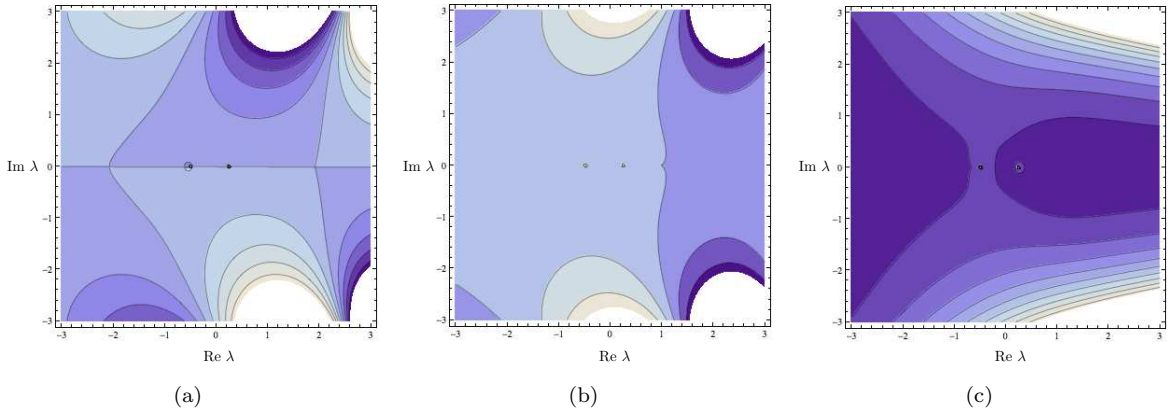


Figure 12: A genus-two Baker–Akhiezer function. Darker shades indicate smaller values. (a) The real part of $\Psi_-$. (b) The imaginary part of $\Psi_-$. (c) The modulus of $\Psi_-$.

and the unnormalized differentials $u_k$. The $a$ periods of these differentials are computed using Chebyshev polynomials and the normalized basis $\omega_k$ is constructed. Next, one point in each $a$-cycle is chosen to be a pole of the BA function. These points make up the divisor for the poles of the BA function. The Abel map of this divisor is computed, along with the Abel map of the divisor

$$D = \sum_{j=1}^{g} (\beta_j, 0).$$

Through the process just outlined the constants $t_j$, $j = 1, \ldots, g$ are computed. The Riemann–Hilbert formulation is used to compute the function $(\Psi_r)_\pm$ by noting that its asymptotic behavior is (6.5). The function $\mathbf{\Sigma}_3$ is found and $u(x,t)$ is computed using Theorem 6.1.

In this section we plot numerical solutions of the KdV equation. In the genus two case we use numerical tests to demonstrate uniform spectral convergence.

### 7.4.1 Genus one

For a genus one solution we set $\alpha_1 = 0, \beta_1 = .25$ and $\alpha_2 = 1$ with the zero of the BA function at $(.5, \sqrt{P(.5)}^+)$ at $t = 0$. See Figure 13 for plots of the corresponding solution of the KdV equation. This solution is an elliptic function. Explicitly, [5],

$$u(x,t) = -\alpha_2 - \beta_1 + 2\,\mathrm{cn}^2(x - K(1-\beta_1) + 1.0768 - (8(1-\beta)^2 - 4 - \alpha_2 - \beta_1)t, 1-\beta_1),$$

where $K(k)$ is the complete elliptic integral and cn is the Jacobi cn function [19]. The shift inside the cn function is computed numerically. See Figure 13 for another solution.

### 7.4.2 Genus two

For a genus two solution we set $\alpha_1 = 0, \beta_1 = .25, \alpha_2 = 1, \beta_2 = 1.5$ and $\alpha_3 = 2$ with the zeros of the BA function at $(.5, \sqrt{P(.5)}^+)$ and $(1.75, \sqrt{P(1.75)}^+)$ at $t = 0$. See Figure 15 for plots of the corresponding solution of the KdV equation.

For this solution we numerically discuss convergence. We use $u_n(x,t)$ to denote the approximate solution of the KdV equation obtained with $n$ collocation points per contour of the RHP. We define the Cauchy error

$$E_{n,m}(x,t) = |u_n(x,t) - u_m(x,t)|.$$

We fix $m = 80$ and let $n$ vary: $n = 10, 20, 40$. See Figure 14 for plots of $E_{n,m}(x,t)$ for various values of $x$ and $t$. This figure demonstrates uniform spectral Cauchy convergence of the function $u_n(x,t)$ to $u(x,t)$, the solution of the KdV equation.

We plot another genus two solution in Figure 15. If we shrink the widths of the bands we can obtain solutions which are closer to the soliton limit. See Figure 16 for a solution demonstrating a soliton-like interaction.

### 7.4.3 Genus three

For a genus three solution we set $\alpha_1 = 0, \beta_1 = .25, \alpha_2 = 1, \beta_2 = 2, \alpha_3 = 2.5, \beta_3 = 3$ and $\alpha_4 = 3.5$ with the zeros of the BA function at $(.5, \sqrt{P(.5)}^+)$, $(1.75, \sqrt{P(1.75)}^+)$ and $(2.75, \sqrt{P(2.75)}^+)$ at $t = 0$. In Figure 17 we show the jump contours for the RHP which are used in practice to compute the BA function. See Figure 19 for plots of the corresponding solution of the KdV equation and Figure 18 and Figure 19 for another genus three solution. We show the dynamics of the zeros of the BA function in Figure 18.

### 7.4.4 Genus five

Just to demonstrate the breadth of the method we compute a genus five solution. We set $\alpha_1 = 0, \beta_1 = .25, \alpha_2 = 1, \beta_2 = 2, \alpha_3 = 2.5, \beta_3 = 3, \alpha_4 = 3.3, \beta_4 = 3.5, \alpha_5 = 4, \beta_5 = 5.1$ and $\alpha_6 = 6$ with the zeros of the BA function at $(.5, \sqrt{P(.5)}^+)$, $(2.2, \sqrt{P(2,2)}^+)$, $(3.2, \sqrt{P(3.2)}^+)$, $(3.6, \sqrt{P(3.6)}^+)$ and $(5.3, \sqrt{P(5.3)}^+)$ at $t = 0$. See Figure 20 for a plot of the corresponding solution of the KdV equation. This figure shows the time evolution.

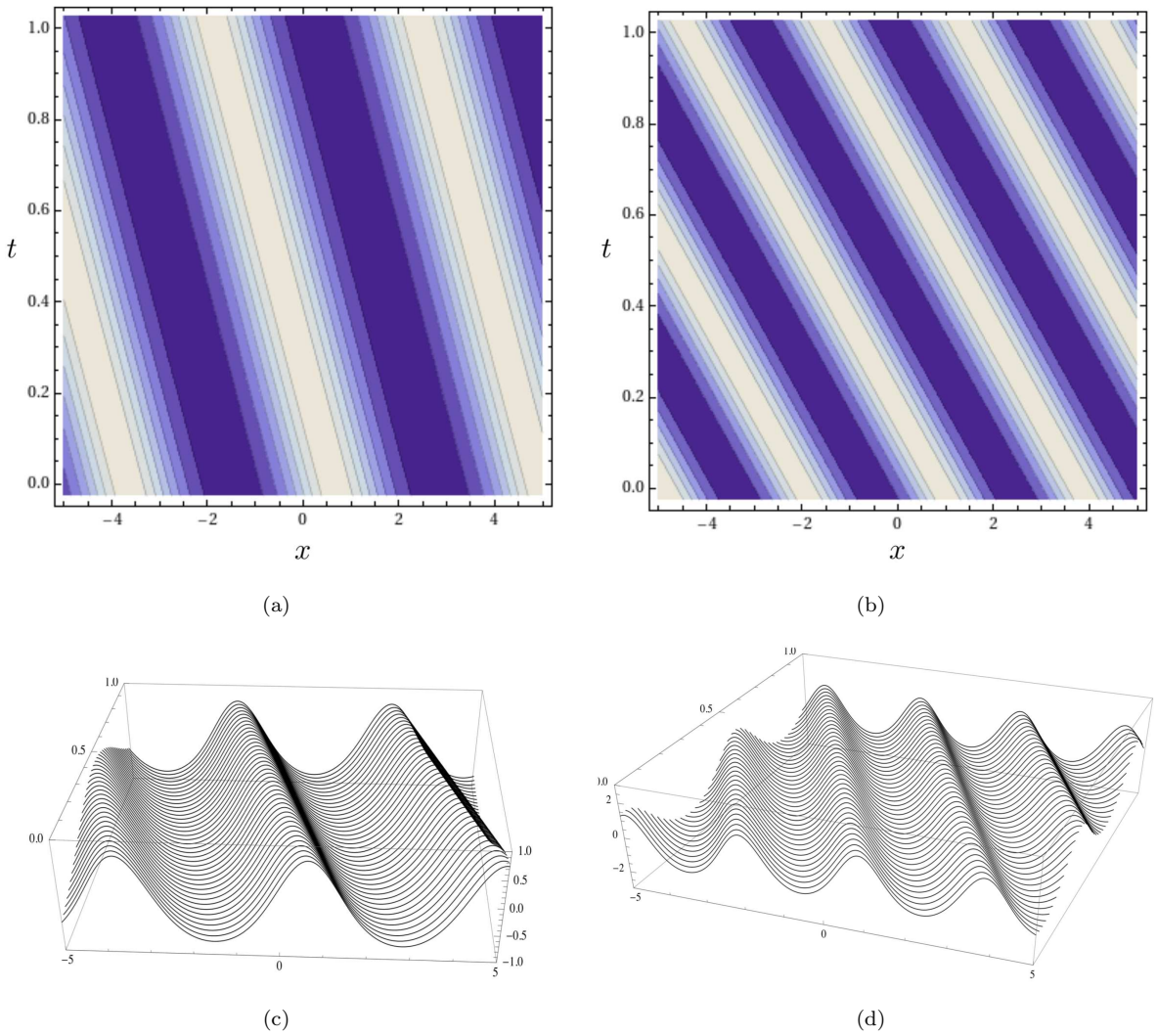


Figure 13: (a) A contour plot of the genus one solution with $\alpha_1 = 0, \beta_1 = .64$ and $\alpha_2 = 1$ with the zero of the BA function at $(.75, \sqrt{P(.75)}^{+})$ at $t = 0$. Darker shades represent troughs. (b) A contour plot of the genus one solution with $\alpha_1 = 0, \beta_1 = .64$ and $\alpha_2 = 1$ with the zero of the BA function at $(.75, \sqrt{P(.75)}^{+})$ at $t = 0$. Again, darker shades represent toughs. (c) A three-dimensional plot of the solution in (a) showing the time evolution. (d) A three-dimensional plot of the solution in (b) showing the time evolution.

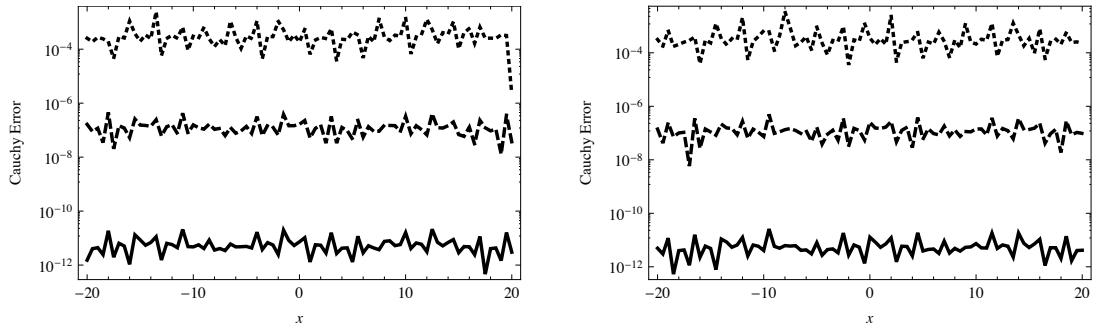


(a) (b)

Figure 14: (a) A logarithmically scaled plot of $E_{n,80}(x,0)$ for $n = 10$ (dotted), $n = 20$ (dashed) and $n = 40$ (solid). (b) A logarithmically scaled plot of $E_{n,80}(x,25)$ for $n = 10$ (dotted), $n = 20$ (dashed) and $n = 40$ (solid). This figure demonstrates uniform spectral convergence.

# 8 Conclusions

We have constructed a method to characterize all Baker–Akhiezer functions which arise from finite-genus solutions of the KdV equation in terms of a classical Riemann–Hilbert problem with smooth solutions. The computational cost to compute the solution to the KdV equation to desired accuracy is seen to be independent of $x$ and $t$.

# Acknowledgments

Support by the National Science Foundation is acknowledged through grant NSF-DMS-1008001 (BD,TT). Any opinions, findings, and conclusions or recommendations expressed in this material are those of the authors and do not necessarily reflect the views of the funding sources.

# A Analysis of the deformed and regularized RHP

In general we consider a RHP form

$$\Phi^+(\lambda) = \Phi^-(\lambda)G(\lambda), \quad \lambda \in \Lambda, \quad \Phi(\infty) = I, \tag{A.1}$$

where $\Lambda$ is bounded and $G$ depends on $\{\Omega_j(x,t)\}_{j=1}^g$, or alternatively $\{W_j(x,t)\}_{j=1}^g$. We follow [25, 26] (see also [21]). We start with a few definitions. Given a self-intersecting piecewise smooth, oriented and bounded contour $\Lambda \subset \mathbb{C}$ define $\gamma_0$ to be the set of self intersections. Define the Cauchy integral of a function defined on $\Lambda$

$$\mathcal{C}_\Lambda f(\lambda) = \frac{1}{2\pi i}\int_\Lambda \frac{f(s)}{s-\lambda}ds, \quad \lambda \notin \Lambda.$$

For $\lambda \notin \gamma_0$ we define

$$\mathcal{C}^\pm_\Lambda f(\lambda) = \lim_{\epsilon\to 0^\pm} \frac{1}{2\pi i}\int_\Lambda \frac{f(s)}{s-(\lambda \pm \epsilon\eta(\lambda))}ds,$$

where $\eta$ is the positive unit normal to $\Lambda$. It is well known that this limit exists for almost every $\lambda$ and the corresponding operators are bounded from $L^2(\Lambda)$ to itself [6, 16]. A matrix-valued function $G : \Lambda \to \mathbb{C}^{2\times 2}$ is said to be in $H^k(\Lambda)$ if it is an $H^k$ function when restricted to each non-self-intersecting component of $\Lambda$. Here $H^k$ refers to the $k$-order $L^2$-based Sobolev space, see [1, 21].

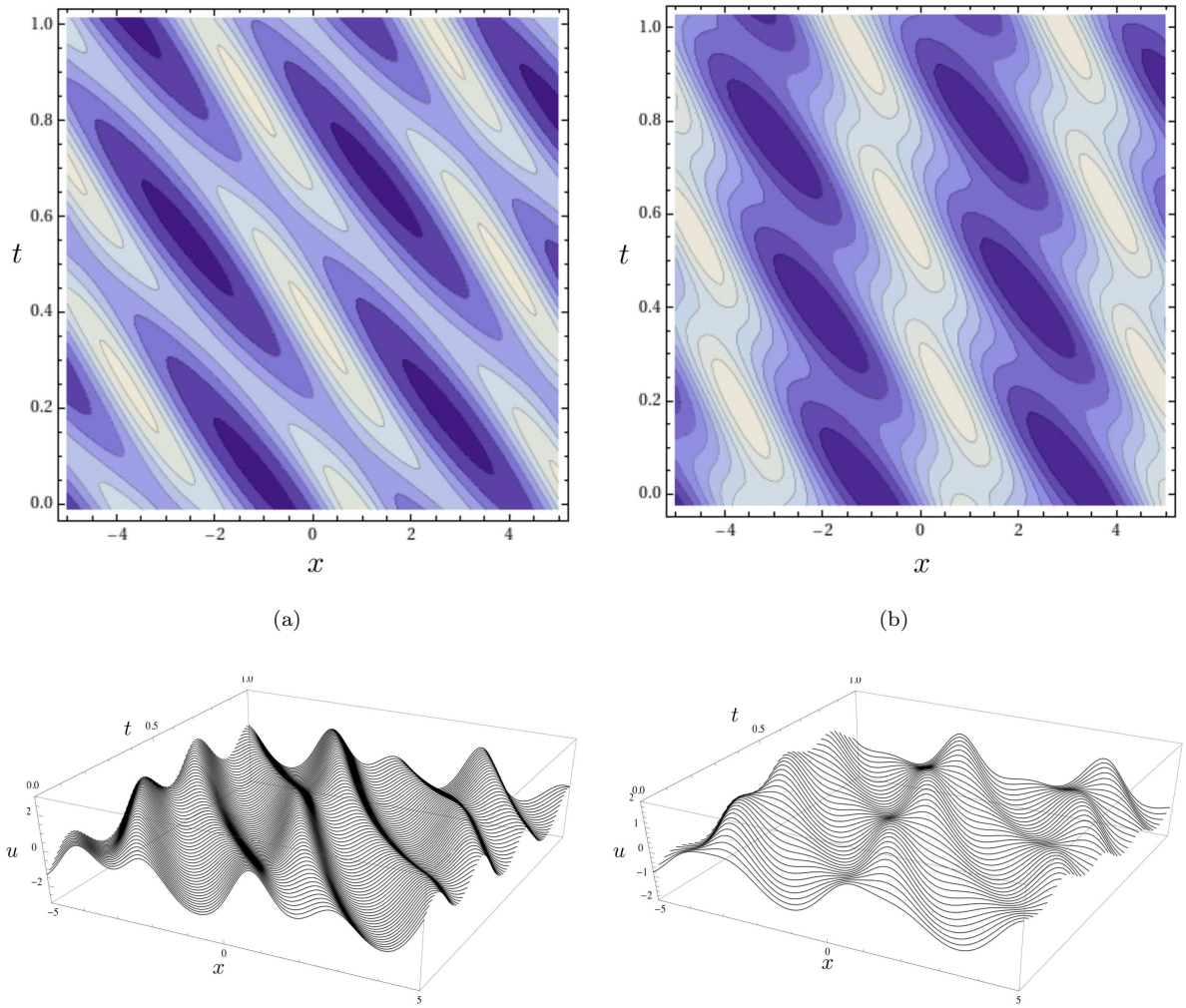


Figure 15: (a) A contour plot of the genus two solution with $\alpha_1 = 0, \beta_1 = .25, \alpha_2 = 1, \beta_2 = 1.5$ and $\alpha_3 = 2$ with the zeros of the BA function at $(.5, \sqrt{P(.5)}^{+})$ and $(1.75, \sqrt{P(1.75)}^{+})$ at $t = 0$. Darker shades represent troughs. (b) A contour plot of the genus two solution with $\alpha_1 = 0, \beta_1 = .25, \alpha_2 = 1, \beta_2 = 2$ and $\alpha_3 = 2.25$ with the zeros of the BA function at $(.5, \sqrt{P(.5)}^{+})$ and $(2.2, \sqrt{P(2.2)}^{+})$ at $t = 0$. Again, darker shades represent toughs. (c) A three-dimensional plot of the solution in (a) showing the time evolution. (d) A three-dimensional plot of the solution in (b) showing the time evolution.

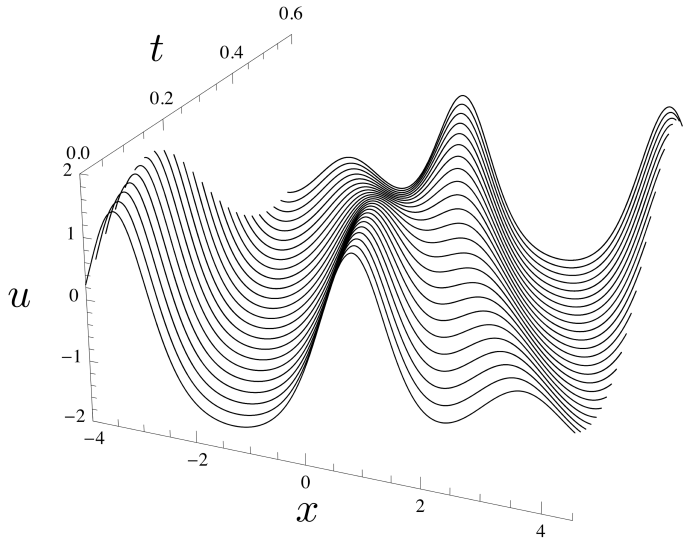


Figure 16: A genus two solution with $\alpha_1 = 0, \beta_1 = 0.1, \alpha_2 = 1, \beta_2 = 1.05$ and $\alpha_3 = 1.75$ with the zeros of the BA function at $(.5, \sqrt{P(.5)}^{+})$ and $(1.2, \sqrt{P(1.2)}^{+})$ at $t = 0$. This solution demonstrates a soliton-like interaction.

**Definition A.1.** *Assume $\lambda_0 \in \gamma_0$ and $G \in H^k(\Lambda)$. Let $\Lambda_1, \ldots, \Lambda_m$ be a counter-clockwise ordering of subcomponents of $\Lambda$ which contain $\lambda = \lambda_0$ as an endpoint. We define $\hat{G}_i$ by $G|_{\tilde{\Lambda}_i}$ if $\Lambda_i$ is oriented outwards and $(G|_{\Lambda_i})^{-1}$ otherwise. We say $G$ satisfies the $(k-1)$th-order product condition if using the $(k-1)$th-order Taylor expansion we have*

$$\prod_{i=1}^{m} \hat{G}_i = I + \mathcal{O}\left((\lambda - \lambda_0)^k\right), \text{ for } j = 1, \ldots, k-1, \quad \forall \lambda_0 \in \gamma_0. \tag{A.2}$$

**Definition A.2.** *Assume that $\lambda_0 \in \gamma_0$ and let $\Lambda_1, \ldots, \Lambda_m$ be a counter-clockwise ordering of subcomponents of $\Lambda$ which contain $\lambda = \lambda_0$ as an endpoint. For $f \in H^k(\Lambda)$, define*

$$f_l^{(j)} = \begin{cases} -\lim_{\lambda \to \lambda_0} \left(\frac{d}{d\lambda}\right)^j f|_{\Lambda_l}(\lambda) & \text{if } \Lambda_l \text{ is oriented outward,} \\ \lim_{z \to \lambda_0} \left(\frac{d}{d\lambda}\right)^j f|_{\Lambda_l}(\lambda) & \text{if } \Lambda_l \text{ is oriented inward.} \end{cases} \tag{A.3}$$

*We say that $f$ satisfies the $(k-1)$th-order zero-sum condition if*

$$\sum_{l=1}^{m} f_l^{(j)} = 0, \text{ for } j = 0, \ldots, k-1 \text{ and } \forall \lambda_0 \in \gamma_0. \tag{A.4}$$

*We use the notation $H_z^k(\Lambda)$ to denote the closed subspace of $H^k(\Lambda)$ consisting of functions that satisfy the $(k-1)$th-order zero-sum condition.*

A contour is said to be complete if $\mathbb{C} \setminus \Lambda = \Omega_+ \cup \Omega_-$ where $\Omega_+ \cap \Omega_- = \varnothing$ and $\Omega_\pm$ lies to the left (right) of $\Lambda$. A contour can always be augmented to a complete contour and matrix-valued functions can be extended to be the identity on these added contours.

**Proposition A.1.** *[26] Let $\Lambda$ be a complete contour and $G \in H^k(\Lambda)$. Assume that $G$ satisfies the $(k-1)$th-order product condition. Then $G$ has an algebraic factorization*

$$G = G_-^{-1} G_+,$$

*such that $G_\pm \in H_z^k(\partial\Omega_\pm)$.*

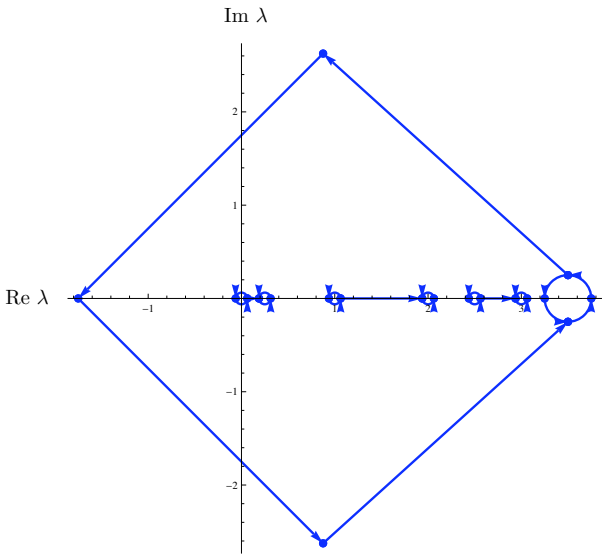


Figure 17: The jump contours for the RHP which are used in practice to compute the BA function. Here $\alpha_1 = 0, \beta_1 = .25, \alpha_2 = 1, \beta_2 = 2, \alpha_3 = 2.5, \beta_3 = 3$ and $\alpha_4 = 3.5$.

This results in the following theorem.

**Theorem A.1.** *[26] The operator $I - C_{G_\pm}$ defined by*

$$(I - C_{G_\pm})u = \mathcal{C}_\Lambda^+[u(I - G_-)] - \mathcal{C}_\Lambda^-[u(I - G_+)]$$

*is Fredholm on $H_z^k(\partial\Omega_+) \cap H_z^k(\partial\Omega_-)$ and has Fredholm index*

$$\operatorname{ind}(I - C_{G_\pm}) = -\frac{1}{\pi i}\left(\int_\Lambda d\log\det G_+ - \int_\Lambda d\log\det G_-\right).$$

*Furthermore, $\Phi = I + \mathcal{C}_\Lambda[\mu(G_+ - G_-)]$, $\Phi : \Lambda \to \mathbb{C}^{2\times 2}$, is a solution of the RHP*

$$\Phi^+ = \Phi^- G, \text{ on } \Lambda, \ \Phi(\infty) = I,$$

*if $\mu$ is a solution of $(I - C_{G\pm})\mu = I$.*

If we partition $\Lambda = \Lambda_1 \cup \cdots \cup \Lambda_m$ into its non-self-intersecting smooth components we obtain

$$\begin{aligned}\operatorname{ind}(I - C_{G_\pm}) &= -2\sum_{l=1}^m \left(\int_{\Lambda_l} d\log\det G_+ - \int_{\Lambda_l} d\log\det G_-\right) \\ &= -2\sum_{l=1}^m \int_{\Lambda_l} d\log\frac{\det G_+}{\det G_-} = -2\sum_{l=1}^m \int_{\Lambda_l} d\log\det G.\end{aligned}$$

We apply this result to the RHP derived in Section 6. We use $G$ to denote the jump matrix. We note that when we augment the contour, $G = I$ on all added pieces and these do not contribute to the integral. Also, $\det \boldsymbol{\Delta} = 1$ away from $\alpha_j$, $\beta_j$ and $\det \boldsymbol{J}_0 = -1$. Both of these do not influence the index. We are left with

$$\begin{aligned}\operatorname{ind}(I - C_{G_\pm}) = -\frac{1}{\pi i}\sum_{l=1}^g \left(\int_{C_{\alpha_l}} d\log\det \boldsymbol{A}_l(\lambda) + \int_{c_{\beta_l}} d\log\det \boldsymbol{B}_l(\lambda)\right) \\ -\frac{1}{\pi i}\int_{\partial\mathcal{D}} d\log\det \boldsymbol{H}(\lambda) - \frac{1}{\pi i}\int_{C_{\alpha_{g+1}}} d\log\det \boldsymbol{A}_{g+1}(\lambda).\end{aligned}$$

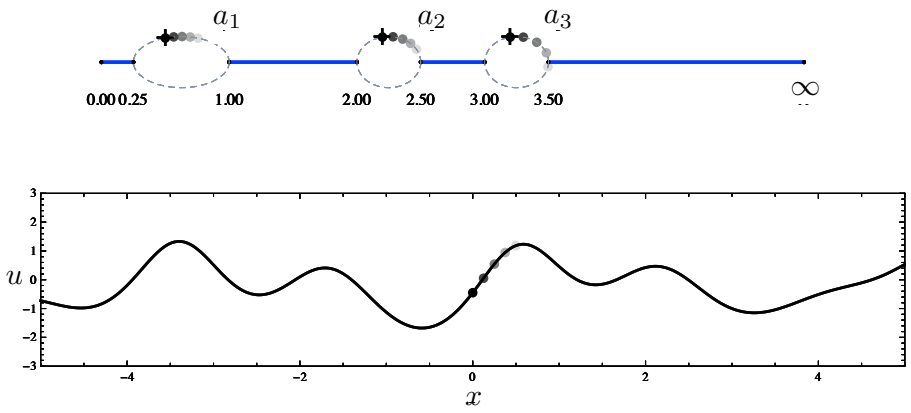


(a)

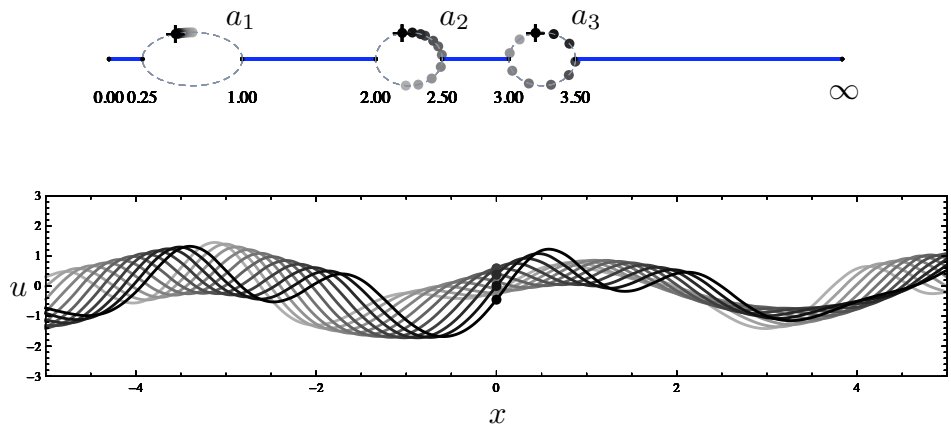


(b)

Figure 18: A genus three solution with $\alpha_1 = 0, \beta_1 = .25, \alpha_2 = 1, \beta_2 = 2, \alpha_3 = 2.5, \beta_3 = 3$ and $\alpha_4 = 3.5$ with the zeros of the BA function at $(.5, \sqrt{P(.5)}^{+}), (2.2, \sqrt{P(2.2)}^{+})$ and $(3.2, \sqrt{P(3.2)}^{+})$ at $t = 0$. These plots show the dynamics of the zeros of the BA function. The top plot in each panel gives a schematic of the Riemann surface with the $a$ cycles labeled. Dots of the same shade across the panels are in correspondence. The $+$ on the plots represents where the pole of the BA function is located on the Riemann surface. These points are also the locations of the zeros at $t = 0$. (a) The solution at $t = 0$. We vary $x$ from $x = 0$ up to $x = 0.25$ and plot how the zeros $\{\gamma_1(x, 0), \gamma_2(x, 0), \gamma_3(x, 0)\}$ move on the Riemann surface. (b) The evolution of the same solution up to $t = 0.125$. We fix $x = 0$ and plot how the zeros $\{\gamma_1(0, t), \gamma_2(0, t), \gamma_3(0, t)\}$ move on the Riemann surface.

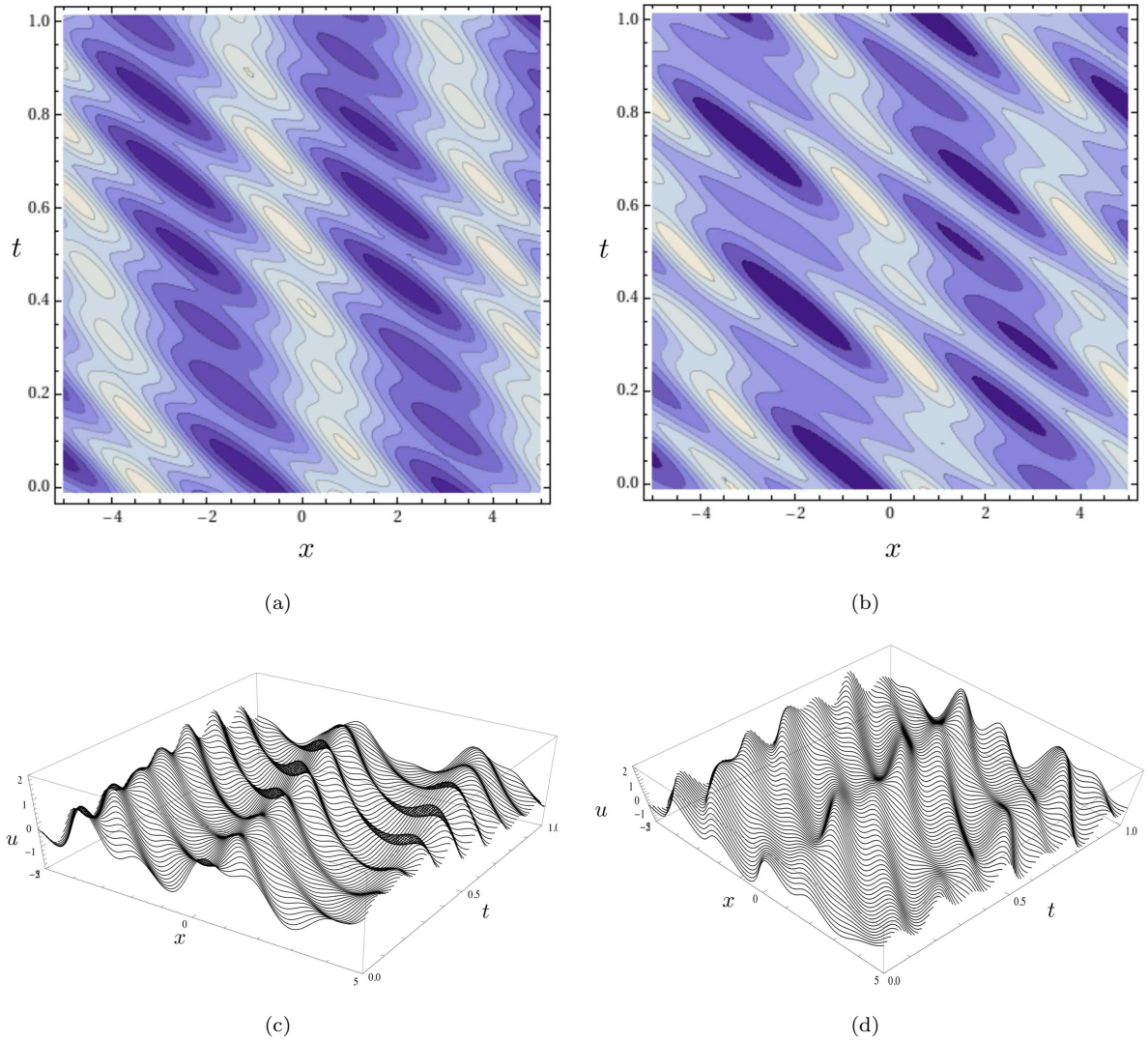


Figure 19: (a) A contour plot of the genus three solution with $\alpha_1 = 0, \beta_1 = .25, \alpha_2 = 1, \beta_2 = 2, \alpha_3 = 2.5, \beta_3 = 3$ and $\alpha_4 = 3.5$ with the zeros of the BA function at $(.5, \sqrt{P(.5)^+}), (2.2, \sqrt{P(2.2)^+})$ and $(3.2, \sqrt{P(3.2)^+})$ at $t = 0$. Darker shades represent troughs. (b) A contour plot of the genus three solution in Figure 18. Again, darker shades represent toughs. (c) A three-dimensional plot of the solution in (a) showing the time evolution. (d) A three-dimensional plot of the solution in Figure 18 showing the time evolution.

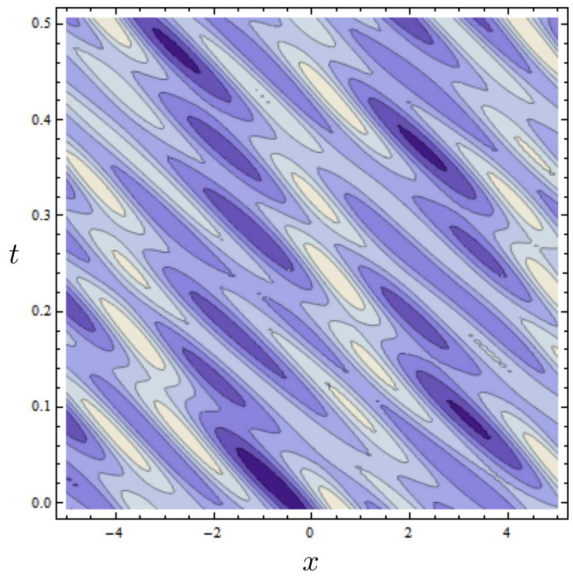


(a)

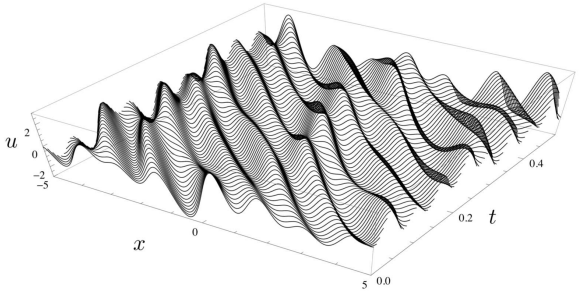


(b)

Figure 20: (a) A contour plot of the genus five solution with $\alpha_1 = 0, \beta_1 = .25, \alpha_2 = 1, \beta_2 = 2, \alpha_3 = 2.5, \beta_3 = 3, \alpha_4 = 3.3, \beta_4 = 3.5, \alpha_5 = 4, \beta_5 = 5.1$ and $\alpha_6 = 6$ with the zeros of the BA function at $(.5, \sqrt{P(.5)}^{+})$, $(2.2, \sqrt{P(2,2)}^{+})$, $(3.2, \sqrt{P(3.2)}^{+})$, $(3.6, \sqrt{P(3.6)}^{+})$ and $(5.3, \sqrt{P(5.3)}^{+})$ at $t = 0$. Darker shades represent troughs. (b) A three-dimensional plot of the solution same solution showing the time evolution.

Here $C_{\alpha_j}, C_{\beta_j}$ are the circles around $\alpha_j, \beta_j$, and $\mathcal{D}$ is again the region inside the large outer circle but outside each of the smaller circles, as before. Straightforward contour integration produces

$$\int_{C_{\alpha_l}} d\log\det \boldsymbol{A}_l(\lambda) = \pi i,$$
$$\int_{C_{\beta_l}} d\log\det \boldsymbol{B}_l(\lambda) = -\pi i,$$
$$\int_{\partial\mathcal{D}} d\log\det \boldsymbol{H}(\lambda) = -\pi i.$$

This proves that $\mathrm{ind}(I - C_{G_\pm}) = 0$. Every element in the kernel of $I - C_{G\pm}$ corresponds to a solution of the RHP that vanishes at infinity [26]. Given a matrix-valued solution $\Phi$, we sum the rows to get the vector representation of the BA function. If we have a vanishing solution we zero out the second row and assume the first is non zero. Call the new function $\Psi$. This is still a vanishing solution. Then $\Phi + c\Psi$ is a solution of the RHP for any $c$. Summing the rows of $\Phi + c\Psi$ we obtain a function different from $\Phi$ for every $c$. This contradicts the uniqueness of the BA function gives that $I - C_{G_\pm}$ must be boundedly invertible by the open mapping theorem. This shows that all RHPs considered here are uniquely solvable with smooth solutions. This is the justification needed to use the numerical method for RHPs in [20].

# B Numerical details and uniform approximation

We consider the RHP (A.1). We use $C$ to denote a generic constant. In this section we explain how our approximation of the BA function changes with $x$ and $t$. We use the results from [21]. For numerical purposes we consider the operator $\mathcal{C}[G;\Lambda]$ defined by

$$\mathcal{C}[G;\Lambda]U = U - (\mathcal{C}_\Lambda^- U)(G - I). \tag{B.1}$$

The operator equation

$$\mathcal{C}[G;\Lambda]U = \begin{bmatrix} 1 & 1 \end{bmatrix}(G - I),$$

is discretized using the method in [20]. We use $\mathcal{C}_n[G;\Lambda]$ to denote this discretization. Once an approximation $U_n$ to $U$ is known, an approximate solution $\Phi_n(\lambda) = \mathcal{C}_\Lambda U_n(\lambda) + \begin{bmatrix} 1 & 1 \end{bmatrix}$ of $\Phi$ is obtained. The method considered is a collocation method and $\Phi_n$ will satisfy the RHP exactly at each collocation point. The residue of a function at $\infty$ is computed through

$$\lim_{\lambda\to\infty} \lambda(\Phi(\lambda) - \begin{bmatrix} 1 & 1 \end{bmatrix}) = -\frac{1}{2\pi i}\int_\Lambda U(s)ds.$$

This is what is used to compute $s_1$ and $s_2$ in (6.4). We make a fundamental assumption.

**Assumption B.1.** *For the problems we consider the following holds:*

$$\|\mathcal{C}_n[G;\Lambda]^{-1}\|_{\mathcal{L}(Y_n,X_n)} \le C(\Lambda)n^l\|\mathcal{C}[G;\Lambda]^{-1}\|_{\mathcal{L}(L^2(\Lambda))}, \quad l \ge 0,$$

*where $X_n$ and $Y_n$ are spaces of mapped Chebyshev polynomials with the $L^2$ norm [21].*

We establish two claims:

- $\|\mathcal{C}[G;\Lambda]^{-1}\|_{\mathcal{L}(L^2(\Lambda))} < C$ and
- $\|G - I\|_{W^{k,\infty}(\Lambda)} < D_k$ for each $k > 0$ for constants $D_k$.

Here $W^{k,\infty}(\Lambda)$ is the $k$th-order $L^\infty$-based Sobolev space [1, 21].

The operator $I - C_{G_\pm}$ depends on $g$ constants $\Omega_j \in [0, 2\pi)$, $j = 1, \ldots, g$ in an analytic way. In the notation of Section A. It follows that the mapping

$$\boldsymbol{\Omega} = (\Omega_1, \ldots, \Omega_j) \mapsto I - C_{G_\pm},$$

is continuous from $[0,2\pi)^g$ to $\mathcal{L}(H^k(\partial\Omega_+)\cap H^k(\partial\Omega_-))$. Since the operator is always invertible the same statement holds for the inverse operator. This implies

$$\sup_{\mathbf{\Omega}} \|I - C_{G_\pm}\|_{\mathcal{L}(H^k(\partial\Omega_+)\cap H^k(\partial\Omega_-))} < C.$$

It is important to note that the operator in (B.1) is different from $I - C_{G_\pm}$. While a solution of one can be mapped to a solution of the other, the operator norms do not share a clear relationship. What we do know is that the solution $\Phi$ of the RHP will satisfy a similar bound:

$$\sup_{\mathbf{\Omega}} \|\Phi^\pm\|_{H^k(\partial\Omega_+)\cap H^k(\partial\Omega_-)} < C. \tag{B.2}$$

Once the unique solution of the RHP is known the inverse of the operator in (B.1) can be written down [21]:

$$\mathcal{C}[G;\Lambda]^{-1}U = \mathcal{C}^+_\Lambda[U\Phi^+][\Phi^{-1}]^+ - \mathcal{C}^-_\Lambda[U\Phi^+][\Phi^{-1}]^-. \tag{B.3}$$

The uniform boundedness of $\Phi^\pm$ in $H^1(\partial\Omega_+)\cap H^1(\partial\Omega_-)$ implies the uniform boundedness of (B.3) as an operator on $L^2(\Lambda)$. This establishes the first claim.

The second claim can be established by differentiating the jump matrix $G$. It is clear that all derivatives of $G$ are bounded and this bound can be made independent of $\mathbf{\Omega}$. This leads to the following theorem which shows we expect uniform spectral convergence of all needed functions.

**Theorem B.1.** *If Assumption B.1 holds then $\Phi_n$, the approximate numerical solution of $\Phi$, satisfies*

$$\sup_{\mathbf{\Omega}} |\Phi_n(\lambda) - \Phi(\lambda)| < C_\alpha \epsilon^{-1} n^{-\alpha}, \quad \textit{for every } \alpha \geq 0, \ \inf_{s\in\Lambda} |\lambda - s| > \epsilon,$$
$$\sup_{\mathbf{\Omega}} \|U_n - U\|_{L^2(\Lambda)} < L_\alpha n^{-\alpha}, \quad \textit{for every } \alpha \geq 0.$$

*As a consequence, the approximate solution $u_n(x,t)$ of the KdV equation satisfies*

$$\sup_{\mathbf{\Omega}} |u_n(x,t) - u(x,t)| < S_\alpha n^{-\alpha}, \quad \textit{for every } \alpha \geq 0.$$

# References


[1] R. A. Adams and J. J. F. Fournier. *Sobolev Spaces.* Academic Press, 2003.

[2] E. D Belokolos, A. I. Bobenko, V. Z. Enol'skii, A. R. Its, and V. B. Matveev. *Algebro-Geometric Approach to Nonlinear Integrable Equations.* Springer, 1994.

[3] J. P. Boyd. *Chebyshev and Fourier spectral methods.* Dover Publications Inc., New York, 2001.

[4] B. Deconinck, M. Heil, A. Bobenko, M. van Hoeij, and M. Schmies. Computing Riemann theta functions. *Math. Comp.*, 73:1417–1442, 2004.

[5] B. Deconinck and D. O. Lovit. Data analysis and reduction using stationary solutions of the NLS equation. *Appl. Anal.*, 89:611–626, 2010.

[6] P. Deift. *Orthogonal Polynomials and Random Matrices: a Riemann-Hilbert Approach.* AMS, Providence, RI, 2000.

[7] P. Deift, S. Venakides, and X. Zhou. An extension of the steepest descent method for Riemann-Hilbert problems: the small dispersion limit of the Korteweg-de Vries (KdV) equation. *Proc. Natl. Acad. Sci. USA*, 95:450–454, 1998.

[8] B. A. Dubrovin. Inverse problem for periodic finite zoned potentials in the theory of scattering. *Func. Anal. and Its Appl.*, 9:61–62, 1975.

[9] B. A. Dubrovin. Theta functions and non-linear equations. *Russian Math. Surveys*, 36:11–92, 1981.

[10] B. A. Dubrovin. Integrable Systems and Riemann Surfaces Lecture Notes. `http://people.sissa.it/~dubrovin/rsnleq_web.pdf`, 2009.

[11] A. S. Fokas, A. R. Its, A. A. Kapaev, and V. Y. Novokshenov. *Painlevé Transcendents: the Riemann–Hilbert Approach*. AMS, Providence, RI, 2006.

[12] J. Frauendiener and C. Klein. Hyperelliptic theta-functions and spectral methods: KdV and KP solutions. *Lett. Math. Phys.*, 76:249–267, 2006.

[13] P. D. Lax. Periodic solutions of the KdV equation. *Comm. Pure Appl. Math.*, 28:141–188, 1975.

[14] H. P. McKean. Review of Riemann surfaces of infinite genus by J. Feldman, H. Knörrer and E. Trubowitz. *Bulletin of the AMS*, 42:79–87, 2005.

[15] H. P. McKean and E. Trubowitz. Hill's surfaces and their theta functions. *Bull. Amer. Math. Soc.*, 84:1042–1085, 1978.

[16] Y. Meyer and R. R. Coifman. *Wavelets: Calderón-Zygmund and Multilinear Operators*. Cambridge University Press, New York, NY, 1997.

[17] S. Novikov, S. V. Manakov, L. P. Pitaevskii, and V. E. Zakharov. *Theory of Solitons*. Constants Bureau, New York, NY, 1984.

[18] S. P. Novikov. A periodic problem for the Korteweg-de Vries equation. I. *Functional Analysis and Its Applications*, 8:54–66, 1974.

[19] F. W. J. Olver, D. W. Lozier, R. F. Boisvert, and C. W. Clark. *NIST Handbook of Mathematical Functions*. Cambridge University Press, 2010.

[20] S. Olver. A general framework for solving Riemann–Hilbert problems numerically. Technical report, Maths Institute, Oxford University, 2010.

[21] S. Olver and T. Trogdon. Nonlinear steepest descent and the numerical solution of Riemann–Hilbert problems. *Submitted for publication*, 2012.

[22] A. R. Osborne. *Nonlinear ocean waves and the inverse scattering transform*, volume 97 of *International Geophysics Series*. Elsevier/Academic Press, Boston, MA, 2010.

[23] T. J. Rivlin. *Chebyshev polynomials*. John Wiley & Sons Inc., New York, NY, 1990. From approximation theory to algebra and number theory.

[24] T. Trogdon, S. Olver, and B. Deconinck. Numerical inverse scattering for the Korteweg–de Vries and modified Korteweg–de Vries equations. *Physica D*, 241:1003–1025, 2012.

[25] X. Zhou. The Riemann–Hilbert problem and inverse scattering. *SIAM J. Math. Anal.*, 20:966–986, 1989.

[26] X. Zhou. Riemann–Hilbert problems and integrable systems. *Lectures at MSRI*, 1999.